CHAPTER VI

EXPERIMENTAL RESULTS AND DISCUSSION III: ERBIUM-DOPED FIBER AMPLIFIER WITH OPTICAL REGENERATIVE-FEEDBACK

6.1 INTRODUCTION

Laser oscillators with regenerative feedback are normally treated as regenerative amplifiers or resonant-type amplifier, operating either below or above the laser threshold [1-3]. In such a system, the injected signal experiences regenerative amplification through the circulation in the cavity. To our knowledge, the first regenerative erbium-doped fiber amplifier (EDFA) was demonstrated in 1999 [4]. In that study, it was reported that the superiority of the system over the conventional single-pass configuration is the high gain performance at the near-resonance regime for the small input signal. However, the application of this regenerative amplifier in optical fiber communication is yet to be tested. In CO_2 regenerative amplifier system [2], it has been shown that regenerative amplification is an extremely useful technique to achieve high-power frequency-stabilized laser sources and is efficient as a power amplifier operating in the saturated regime. In this chapter, we demonstrate the characteristics of the regenerative erbium-doped fiber ring amplifier operating both below and above the threshold for self-oscillation. The theory of regenerative amplifier is presented in Appendix B.

The studied is started from the case with the existence of tunable bandpass filter (TBF) in the cavity. Regenerative-feedback is achieved by tuning the input signal to the wavelength of the TBF. This is presented in Sec. 6.3. Different measurement methods were compared again since the phase change due to the circulation of the input signal is expected to affect the collected data. Without the TBF as demonstrated in Sec. 6.4, the system is studied both below and above thresholds of oscillation. Comparison with the system without feedback is presented. Operating above the oscillation threshold, the system is compared with the co-feedback gain-clamped EDFA. Due to the resonant-amplification characteristics of the regenerative amplifier, a flat gain spectral is difficult to achieve. When the regenerative amplifier system is subjected to another external injection, injection-locking and gain enhancement effects are observed. A plausible explanation of the mechanism of the gain enhancement is suggested. Potential application as a high-power frequency-stabilized laser source is proposed based on injection-locking phenomenon. The data is presented in Sec. 6.5 and 6.6, respectively. Finally, a bidirectional-feedback regenerative EDFA is studied by removing the optical isolator from the cavity, leading the laser oscillating in both clockwise and anti-clockwise directions. This studied is demonstrated in Sec. 6.7.

6.2 EXPERIMENTAL SETUP

The configuration for demonstrating the EDFA with regenerative optical feedback is shown in Fig. 6.1. The system consists of two 980/1550 nm wavelength division multiplexers: WDM I and WDM II, two couplers: C_1 and C_2, with an output coupling ratio of 95 %. An optical isolator, ISO 1, was placed in the cavity in co-feedback direction to create a unidirectional regenerative feedback in the oscillator.

This system differs from the typical co-propagating gain-clamped erbium-doped fiber amplifiers (as presented in Chapter V) in which the wavelength filtering element has been omitted, allowing circulation of the injected signal to achieve regenerative amplification. A-15-m long erbium-doped fiber with a cut-off wavelength of 950 nm, a refractive index of 1.473 and an Er^{3+} concentration of +440 ppm was used as an active medium. Pump power was provided by a laser diode from the 980 nm port of WDM I. The signal source was from an ANDO AQ4321D tunable laser source (TLS) set at CW mode and the amplified output signal was monitored using an ANDO AQ6317B set at the resolution of 0.05 nm.

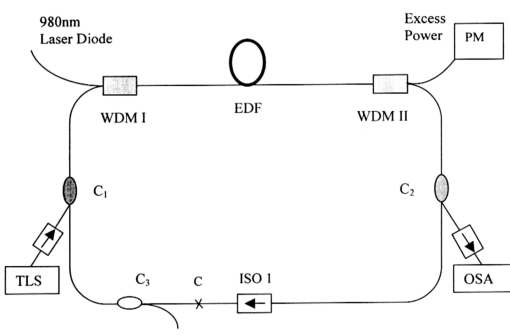

Fig. 6.1 *Experimental setup for demonstrating the regenerative feedback erbium-doped fiber amplifier. (EDF: erbium-doped fiber; WDM: wavelength division multiplexer; $C_{1,\ 2,\ 3}$: coupler; ISO: isolator; PM: power meter; TLS: tunable laser source; OSA: optical spectrum analyzer, C: spiced point to be opened.)*

6.3 UNIDIRECTIONAL-FEEDBACK WITH WAVELENGHT SELECTIVE ELEMENT

6.3.1 Comparison between Different Measurement Methods

In this section, regenerative-feedback EDFA with the wavelength selective element is presented. The signal wavelength was tuned to the wavelength of tunable bandpass filter (TBF), i.e., 1550 nm. Fig. 6.2 (a) shows that with the wavelength of TBF tuned to 1550 nm, there is a potential of lasing mode occurring at the pump power of P_p = 23.8 mW. Injected at the wavelength of λ_{sig} = 1550 nm and the power of P_{in} = -30 dBm as shown in Fig. 6.2(b), the input signal experiences regenerative amplification through the circulation in the cavity.

The data presented in Chapter 4 and Chapter 5 was taken using Time-Domain Extinction (TDE) Method. Since the phase of the input signal is optical path length dependent, it changes after passing through the active medium (EDF) of 15 m in length. Calibration of the phase is one of the processes in the measurement based on the TDE method. In the regenerative-feedback scheme, however, circulation of the signal induces phase perturbation and causes inaccuracy in the data measurement using TDE method. Therefore, comparison is done as a function of pump power between TDE Method and Interpolation Method for such an amplifier scheme.

Signal gain and noise figure were taken for the comparison between two different measurement methods. The data were taken for the pump powers below threshold. Fig. 6.3 shows that the signal gain discrepancy is small for the low pump powers with that obtained from TDE method exhibiting a lower gain. The deviation increases with the pump power. Maximum discrepancy of 2.9 dB is achieved at the maximum pump power P_p = 23.8 mW. Similar to the signal gain, the noise figure (see Fig. 6.4) deviation between two measurement methods also increases with the pump

power with the maximum deviation of 2.9 dB at the pump power P_p = 23.8 mW. It has been shown in Section 3.5.3 in Chapter 3 that the TDE method gives a signal gain (~1 dB) and a noise figure (~0.9 dB) higher than those obtained using interpolation method for the *single-pass EDFA system*. However, with the *circulation* of the input signal in the regenerative-feedback scheme, phase perturbation causes inaccuracy in the measurement using TDE method. To obtain an accurate measurement, interpolation method is thus chosen for the following experiments based on the regenerative-feedback scheme.

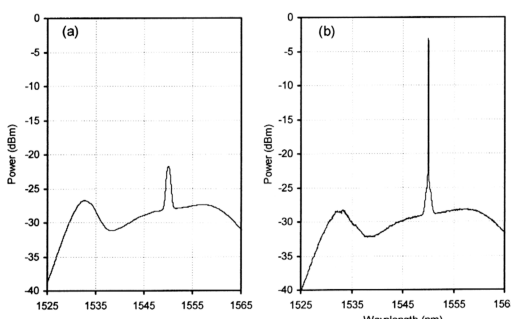

Fig. 6.2 *Output spectrum with TBF tuned to the wavelength of 1550 nm at the P_p = 23.8 mW. (a) Without input signal. (b) With the input signal at P_{in} = -30 dBm.*

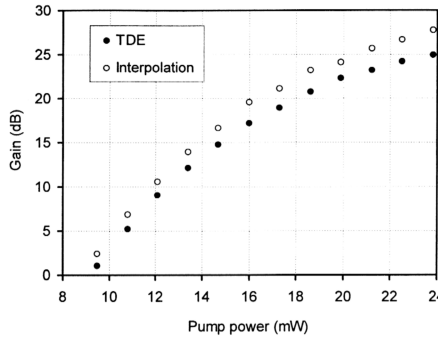

Fig. 6.3 *Signal gain as a function of pump power obtained from TDE and Interpolation methods at P_p = 23.8 mW and P_{in} = -30 dBm.*

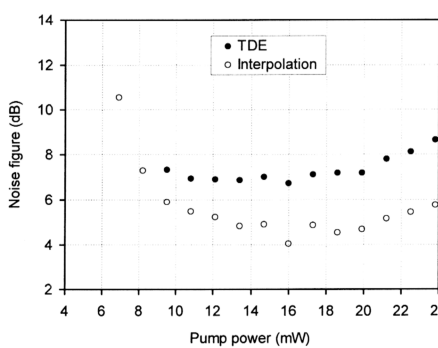

Fig. 6.4 *Noise figure versus pump obtained from TDE and Interpolation methods at P_p = 23.8 mW and P_{in} = -30 dBm.*

6.3.2 Comparison with System Without Feedback

In this section, regenerative-feedback scheme is compared with the system without feedback. The pump power and signal wavelength are P_p = 23.8 mW and λ_{sig} = 1550 nm, respectively. The data was taken as a function of input signal power, P_{in}. Fig. 6.5 shows the signal gain for both schemes. Without the optical feedback, the small-signal gain of 24.3 dB is achieved. By 3-dB gain compression, the saturation input signal power is determined to be P_{in}^{sat} = –19 dBm. At the P_{in} = -42 dBm, the regenerative-feedback scheme exhibits a signal gain by 6.1 dB higher than that achieved by the system without feedback. Through the circulation in the cavity, the input signal experiences regenerative amplification and thus a higher signal gain. A stronger amplification in this case saturates the active medium with an input signal 11 dB lower than the case without feedback.

Noise figure as a function of input signal power P_{in} is illustrated in Fig. 6.6. The noise figures for both systems are almost identical except at the P_{in} from –18 dBm to –32 dBm where the deviation occurs. Such a deviation may arise from the insertion loss inconsistency during plug-in and plug-out of the connectors during the measurement. Note that the dip effect is observed for both systems due to the backward ASE suppression as mentioned earlier in Chapter 4 and 5.

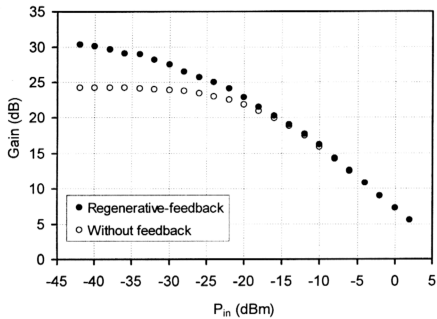

Fig. 6.5 *Signal gain comparison between system with and without regenerative-feedback at $P_p = 23.8$ mW and $\lambda_{sig} = 1550$ nm.*

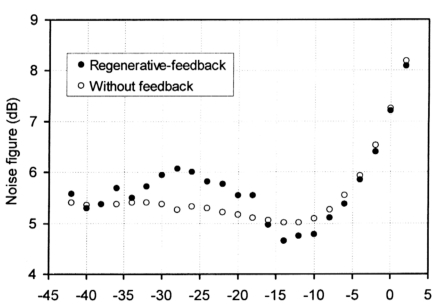

Fig. 6.6 *Noise figure comparison between system with and without regenerative-feedback at $P_p = 23.8$ mW and $\lambda_{sig} = 1550$ nm.*

6.4 UNIDIRECTIONAL-FEEDBACK WITHOUT WAVELENGTH SELECTIVE ELEMENT

6.4.1 Operation Below Threshold

6.4.1.1 Amplifier Performance

Fig. 6.7 shows the output spectrum of the regenerative EDFA at the pump power P_p = 29.4 mW, just below the oscillation threshold. The thick line represents the output spectrum without the input signal. Since the system is pumped just below the oscillation threshold, there is a potential lasing mode at the wavelength of λ_{laser} = 1557.7 nm. By injecting an external signal with a power of P_{in} = -30 dBm at the signal wavelength of λ_{sig} = 1557.7 nm, a significant suppression of the amplified spontaneous emission (ASE) level was observed (represented by thin line). The reduction in the emission spectrum especially at the resonance is thus balanced by the energy needed to provide amplification of the input signal. The inset shows the power suppression in this case. Maximum suppression of 9.5 dB is observed at resonance (zero detuning).

Signal gain as a function of pump power P_p for different P_{in} is denoted in Fig. 6.8. The signal is at the resonant wavelength of λ_o = 1557.7 nm as shown in Fig. 6.7. For the small-signal P_{in} = -40 dBm and –30 dBm, the signal gain increases steeply with the pump power due to the increase in the average population inversion. With this resonant amplification, signal gain as high as 37 dB and 32.3 dB is achieved for P_{in} = -40 dBm and –30 dBm, respectively, at the near-threshold pump power P_p = 29.4 mW. The amplifier is saturated by the strong P_{in} of –10 dBm and 0 dBm. For example, the signal gain is only 8.8 dB for P_{in} = 0 dBm at P_p = 29.4 mW.

Although the pump powers below threshold are low, low noise figure is still achievable in this regenerative amplifier system based on the co-pumping scheme. The data is depicted in Fig. 6.9. With the saturating input signal P_{in} = 0 dBm, depletion of the population at the metastable level at the EDF input end causes the highest noise figure within the given pumping range. Basically, the noise figure decreases with the pump power. A striking feature is that with the small signal of P_{in} = -40 dBm, the noise figure starts to increase from P_p > 20 mW. This can be attributed to the increase in the backward ASE with the pump power that depopulates the inversion at the EDF input end [5-7]. The lowest noise figure of 5.3 dB is achieved at this input signal level at P_p = 17.3 mW. With the other higher P_{in}, the backward ASE is suppressed. In consequence, the inversion level at the EDF input end increases, resulting in decrease in the noise figure with the pump power. Note that at the P_p > 18.6 mW, the noise figure of the input signal with P_{in} = -10 dBm becomes the lowest among different P_{in}. This reveals that the backward ASE is effectively suppressed by this injection level. Noise figure as low as 5.2 dB is achieved at P_p = 29.4 mW. Excluding the input coupling loss of 1.53 dB, noise figure near quantum limit (3.7 dB) is exhibited, indicating a nearly complete inversion at the EDF input end.

With different pump powers, the signal gain is studied as a function of input signal power, P_{in}, as denoted in Fig. 6.10. In the small-signal gain regime, higher signal gain is achieved at the higher pump powers. For example, signal gain as high as 36.8 dB is achievable at P_{in} = -40 dBm for the P_p = 29.4 mW. However, strong amplification results in saturation for the input signal as low as P_{in}^{sat} = –32 dBm. The saturation input power, P_{in}^{sat} can be improved to –21 dBm with a lower P_p = 17.3 mW. It is compensated at a cost of 13.8 dB reduction in the signal gain at P_{in} = -40 dBm. A

linear amplification is only available at this pump power in a limited small-signal regime.

In Fig. 6.11, noise figure versus input signal power for P_p = 17.3 mW, 23.8 mW and 29.4 mW is denoted. With the maximum pump power P_p = 29.4 mw, existence of the strong backward ASE results in self-saturation at the EDF input end. Consequently, noise figure is high in the unsaturated regime particularly for P_{in} > -35 dBm. By increasing the P_{in}, the backward ASE is suppressed and the inversion at the EDF input end is restored back to a higher level. Such an effect is also observed for P_p = 17.3 mW and 23.8 mW. It is evident that at $P_{in} \approx$ -15 dBm, the backward ASE is effectively suppressed for all the cases here since the noise figures are among the lowest. Beyond this P_{in}, signal-induced saturation starts to dominate in the mechanism of the saturation [8].

Signal gain is studied as a function of signal wavelength, λ_{sig} with P_p = 29.4 mW as depicted in Fig. 6.12. With the small input signal P_{in} = -30 dBm, resonance amplification is possible where the gain spectral follows the shape of the ASE spectrum profile. Resonant gain as high as 32.3 dB is achieved with this small signal. The corresponding gain bandwidth, where the gain difference is < 3 dB, is about 10 nm wide. A flatter gain spectral is achievable with the saturating signal P_{in} = -10 dBm. However, the signal gain is degraded to be ~17.7 dB at the resonant wavelength due to the saturation effect induced by the strong signal. A strong saturation effect is observed with P_{in} = 0 dBm. In this case, a flat gain is obtained over the entire amplification bandwidth of study with the maximum gain of 8.7 dB. The maximum gain deviation is 1.4 dB in the given bandwidth.

Fig. 6.13 shows the noise figure versus signal wavelength, λ_{sig} at pump power P_p = 29.4 mW. Low noise figure (~5.5 dB) is achieved with P_{in} = -30 dBm. With the

P_{in} = -10 dBm, a low noise figure (~5.5 dB) is also achievable since this P_{in} is able to effectively suppress the backward ASE at the EDF input end. In the case of P_{in} = 0 dBm, however, signal-induced saturation dominates the amplifier system rather than the backward ASE suppression. Therefore, noise figure > 6.5 dB is exhibited in this case.

The excess pump power monitored from the 980 nm port of WDM II using an optical power meter (ILX Lightwave OMM 6810B) was taken as a function of signal wavelength as shown in Fig. 6.14. The pump power was fixed at P_p = 29.4 mW, just below the oscillation threshold. A constant signal of P_{in} = -30 dBm was applied to the system. The filled circles show the data for the regenerative-feedback scheme. A sinusoidal-like curve is observed. A possible explanation for this is the back reflection arising from the splicing points at both EDF ends. A Fabry-Perot cavity is then formed in the active medium. Such an interference effect arising from this standing-wave feature creates a population modulation or grating [9] along the active medium. Note that the modulation of the excess pump power is gain dependent. The interference effect is strong at the high gain regime around 1558 nm. To prove that the phenomenon was not arisen from the interference between the input signal and the circulating input signal in the clockwise direction, the ring was opened at the point between the coupler C_3 and the isolator, ISO 1. The open circles show the data for the case of open ring.

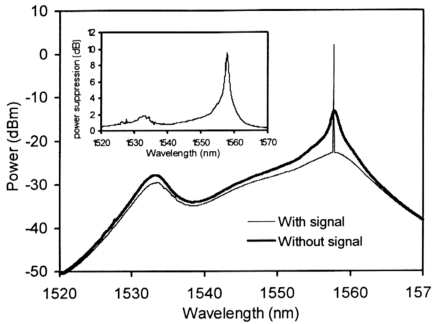

Fig. 6.7 *Output spectrum of the regenerative EDFA at the pump power of 29.4 mW. (Thick line: without input signal; thin line: with input signal at P_{in} = -30 dBm and λ_{sig} = 1557.7 nm). The inset shows the power suppression.*

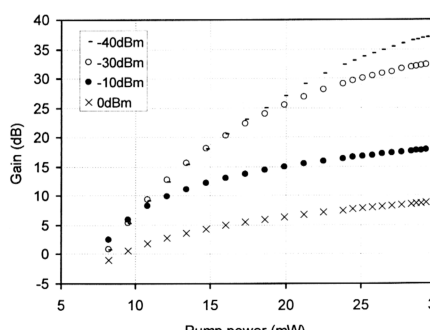

Fig. 6.8 *Signal gain as a function of pump power for different input signal powers.*

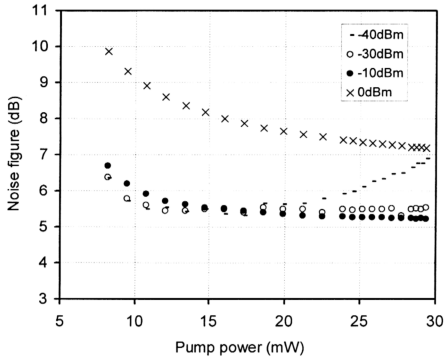

Fig. 6.9 *Noise figure as a function of pump power for different input signal powers.*

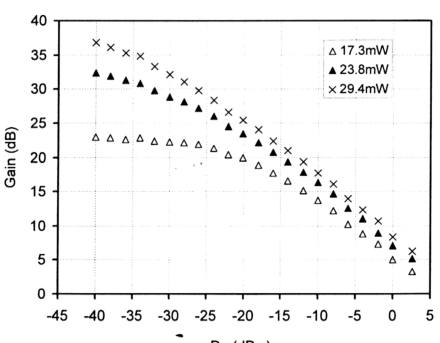

Fig. 6.10 *Signal gain as a function of input signal power for different pump powers.*

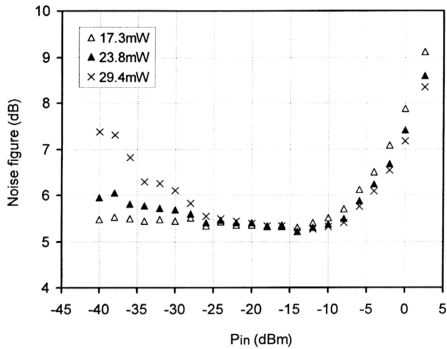

Fig. 6.11 *Noise figure as a function of input signal power for different pump powers.*

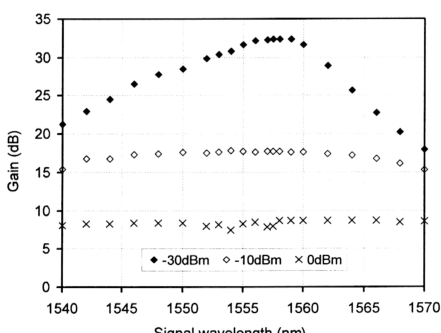

Fig. 6.12 *Signal gain as a function of signal wavelength for different input signal powers.*

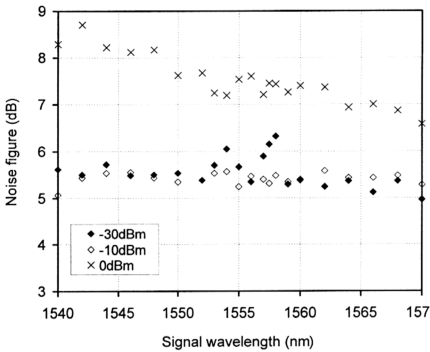

Fig. 6.13 *Noise figure versus signal wavelength for different input signal power.*

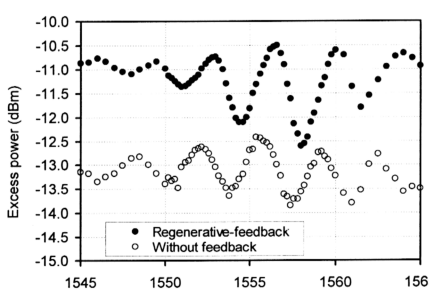

Fig. 6.14 *Excess pump power as a function of signal wavelength at P_p = 29.4 mW.*

6.4.1.2 Saturation Characteristics

Fig. 6.15 shows the signal gain as a function of input signal power, P_{in} for different positive detuning $\Delta\lambda_+ = 0$ nm, 2 nm, 5 nm and 10 nm at the pump power just below the oscillation threshold. The on-resonance signal gain as high as 36.8 dB has been achieved with P_{in} = -40 dBm. The corresponding saturation input power, by 3-dB gain compression, in this case is P_{in}^{sat} = -32.6 dBm. With the injected signal detuned by 2 nm and 5 nm from the resonance, the gain decreases to 34.9 dB and 27.4 dB, respectively. However, the P_{in}^{sat} increases to –30 dBm and –20 dBm, respectively, under this off-resonance condition. By detuning the signal to 10 nm, a larger dynamic range can be obtained. Since 10 nm of detuning is far from the regenerative-amplification regime around the resonance, the small-signal gain is low in this case, i.e., 20.1 dB with the P_{in}^{sat} = –11.5 dBm.

Signal gain as a function of signal detuning, $\Delta\lambda$, for different P_{in} is illustrated in Fig. 6.16. Although the system is operating below the oscillation threshold, it will still amplify signals as long as the gain from the medium exceeds the loss. With a small signal P_{in} = -40 dBm, the gain bandwidth is relatively narrow, following the shape of the output spectrum as shown in Fig. 6.7. The maximum signal gain of 35.1 dB is achieved at zero detuning. Note that the resonant amplification is preserved only for small P_{in}. With the higher input powers such as P_{in} = -30 dBm and –20 dBm, the resonance gains decrease to be almost equal to those of off-resonance with the small detuning. For example, with the P_{in} = -20 dBm, the resonance gain at zero detuning is 25.3 dB, similar to the off-resonance gain at the negative detuning of $\Delta\lambda_-$ = -4 nm. The resonant gain of the amplifier is modified as a result of the saturation characteristics of the gain medium by the strong input signal. Consequently, the gain

bandwidth, which increases with the P_{in}, is also modified by the saturation. Under the condition of small input signal, the effects of saturation are negligible and thus a high resonant amplification is preserved. However, from a practical point of view, such a narrow amplification bandwidth is not well suited for multi-channels amplification purpose if the P_{in} is low. A broader amplification bandwidth is achieved with a relatively higher input signal power as for example around -10 dBm. Although a broad bandwidth at the same wavelength range can be obtained if the amplifier is pumped far below threshold, the signal gain and efficiency would be significantly decreased.

Fig. 6.17 shows the saturated input signal power, P_{in}^{sat} as a function of signal detuning, $\Delta\lambda$. The curve shows an inverse relationship with the output spectrum and gain spectrum with small P_{in}. For the negative detuning, the regenerative amplifier saturates at a lower input power compared to that of the positive detuning. This asymmetrical property is a consequence of asymmetry in the regenerative amplification as shown in Fig. 6.16 where higher signal gains are achieved for the negative detuning. For example, with the input signal power of P_{in} = -40 dBm, the signal gain at negative detuning is ~7 dB higher than that of the same amount of positive detuning. Such a higher circulating power in the cavity results in the saturation of the amplifying medium with a relatively small P_{in} as compared to the case of the positive detuning. The largest discrepancy as compared to the system without feedback is observed at resonance. However, with a large detuning, resonant-amplification of the regenerative amplifier is no longer preserved. Thus, P_{in}^{sat} for both schemes tends to be identical.

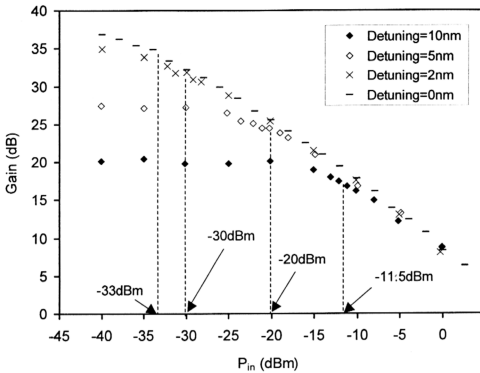

Fig. 6.15 *Signal gain as a function of input signal power, P_{in} for different positive detuning of $\Delta\lambda_+ = 0$ nm, 2 nm, 5 nm and 10 nm.*

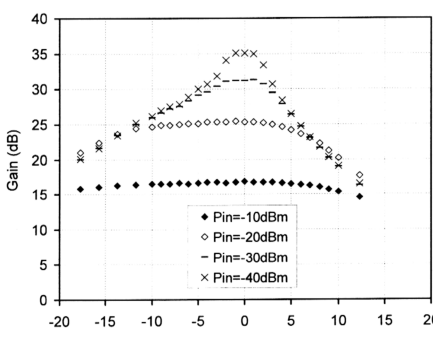

Fig. 6.16 *Signal gain as a function of signal detuning for different input signal powers.*

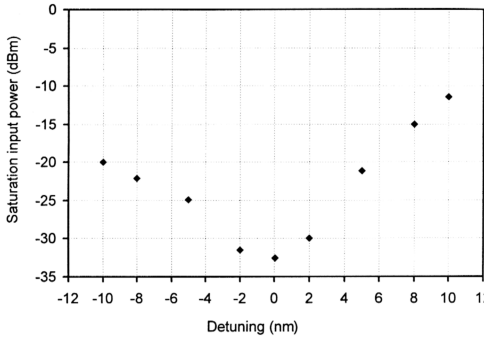

Fig. 6.17 *Saturation input signal power as a function of signal detuning.*

6.4.1.3 Amplification Bandwidth

In this section, saturation-induced variation in the amplification bandwidth is presented. To describe the amplification behavior of the regenerative amplifier, it is necessary to include implicitly the saturation characteristics of the active medium. Fig. 6.18 shows the amplified output powers as a function of signal detuning for P_{in} = -10 dBm, -30 dBm and –40 dBm. With the P_{in} = -40 dBm, resonant amplification is preserved where the signal with a small detuning experiences strong amplification. The amplification bandwidth is narrow in this case. With a higher P_{in}, the amplification bandwidth becomes broader. A flat amplified output power spectrum is obtained with a strong input signal power, and regenerative amplifier system behaves like a conventional single-pass amplifier system where the ASE-like shape is no longer preserved. The resonant amplification characteristic of the regenerative

amplifier is modified as a result of the saturation of the gain medium by the strong input power.

Fig. 6.19 illustrated the signal gain and amplification bandwidth with 3-dB compression (or half-power bandwidth) as a function of the input power P_{in}. In the small-signal gain regime, the amplifier bandwidth is only about 6 nm. At the low input power, saturation can be neglected in the determination of the bandwidth. When P_{in} > -35 dBm, the amplification bandwidth increases significantly. Regenerative-feedback allows the input signal inside the cavity to recirculate inside the cavity many times, extracting energy from the medium in each cycle. As a result, the recirculating signal builds up to a very large amplitude inside the cavity. In the regime of moderate saturation, the amplification bandwidth increases linearly. For these input powers, the circulating signal power within the cavity significantly perturbs the small-signal gain of the active medium.

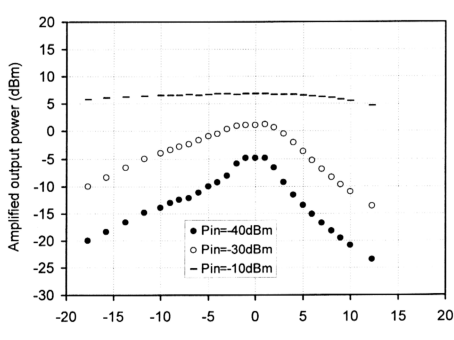

Fig. 6.18 *Amplified output power as a function of signal detuning.*

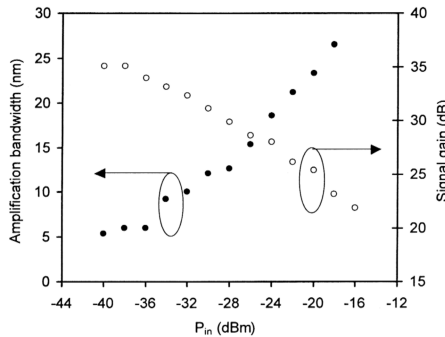

Fig. 6.19 *Signal gain and amplification bandwidth as a function of the input power.*

6.4.1.4 Comparison with the System Without Feedback

In this section, the performance of regenerative-feedback scheme is compared with that of the system without feedback. The ring was opened at the point C in the configuration as shown in Fig. 6.1. To minimize back reflection, index-matching gel was applied to both free fiber ends. With the input signal injected at λ_{sig} = 1557.7 nm and P_{in} = -30 dBm, the data for signal gain as a function of the below threshold pump power P_p is plotted in Fig. 6.20. At the low pump powers, the signal gains are almost identical for both schemes since the amount of the ASE that is being feedback to the system is negligible under this condition. The effect of regenerative-feedback becomes significant at the higher P_p where the discrepancy in the signal gains increases progressively. At P_p = 29.4 mW, just below the oscillation threshold,

regenerative-feedback scheme achieves the signal gain as high as 32.3 dB. For the system without feedback, the maximum achievable signal gain is just 24.9 dB at the same P_p, 7.4 dB lower than that of the former scheme.

Figs. 6.21 (a), (b) and (c) show the pump power dependence of the noise figure for P_{in} = -40 dBm, -30 dBm and –10 dBm, respectively. With the small P_p, the noise figures are high as a result of low inversion level at the EDF input end. In the case of P_{in} = -40 dBm (Fig. 6.21(a)) the regenerative-feedback scheme has the noise figure ~0.5 dB lower for the low P_p as compared to the case without feedback. In the system without feedback, the existing backward ASE cannot be suppressed by this small P_{in}. Therefore, the noise figure is high. However, a small amount of the regenerative-feedback ASE in the clockwise direction is sufficient to suppress the backward ASE, resulting in a smaller noise figure. A striking feature is that at P_p > 17.5 mW, the noise figure starts to increase with P_p. Such a phenomenon can be attributed to the higher depopulation rate induced by the backward ASE at the higher pump powers as compared to the backward ASE suppression rate by the regeneratively feedback light. Another reason is that at the pump power near-threshold, the ASE level P_{ASE} increases progressively. This ASE level contributes to the high noise figure according to Eq. (3.2). With P_{in} = -30 dBm as shown in Fig. 6.21(b), ASE self-saturation at the EDF input end is balanced by the signal-induced backward ASE suppression. It is evident in this case that the noise figures for both schemes are constant for the P_p > 12 mW. The backward ASE can be effectively suppressed with P_{in} = -10 dBm (see Fig. 6. 21(c)). As a result, the inversion level at the EDF input end increases with P_p and thus, the noise figures decrease with P_p.

With the pump power of 29.4 mW, signal gain as a function of input signal power, P_{in} is compared between the schemes as depicted Fig. 6.22. Without the

optical feedback, linear amplification is possible for P_{in} < -30 dBm. The small-signal gain in this unsaturated regime is ~26 dB with the saturation input signal power P_{in}^{sat} = -22 dBm. Different from the system without feedback, the regenerative-feedback scheme saturates even with a small P_{in} (P_{in}^{sat} = -32 dBm) due to the strong regenerative amplification. With the small signal of P_{in} = -40 dBm, signal gain as high as 36.8 dB is achievable. In the moderately saturated regime (P_{in} > -15 dBm) both schemes exhibit the signal gains close to each other. With this high P_{in}, saturation of the active medium causes the regenerative-feedback portion experiences only a small gain. Therefore, the regenerative-feedback scheme behaves like the system without feedback.

Fig. 6.23 shows the noise figure versus input signal power at the pump power P_p = 29.4 mW, just below the threshold of self-oscillation. With this pump power, there is a potential laser mode at wavelength of ~1558 nm as shown in the forward ASE spectrum of Fig. 6.7 for the regenerative amplifier system. At this region, the measured P_{ASE} is high. Basically, injecting a small signal P_{in} ≈ -40 dBm at this wavelength will not significantly change the ASE level. Therefore, the noise figure is high according to Eq. (3.2). Such a high P_{ASE} level can be compressed by increasing the P_{in}. Instead of backward ASE suppression, a higher P_{in} also contributes to decrease in noise figure through compression of P_{ASE} level. Without the feedback, the ASE level is fairly flat at the wavelength ~1558 nm. In consequence, the noise figure is relatively constant in the small-signal regime.

Amplified signal output power, P_{out}, as a function of P_{in} is depicted in Fig. 6.24. In the small-signal regime, the output power increases linearly with the input power. With the existence of the saturation effect, regenerative-feedback scheme

exhibits a smaller slope as compared to the case without feedback. A higher output power, P_{out} can be obtained from the regenerative-feedback scheme in this regime. For the $P_{in} > 0$ dBm, the output powers for both systems are almost identical. The effect of the regenerative-feedback becomes insignificant.

Fig. 6.25 shows the signal gain versus signal detuning, $\Delta\lambda$, at $P_p = 29.4$ mW. The input signal was fixed at $P_{in} = -30$ dBm and detuned from the potential lasing mode of 1557.7 nm. Similar to the conventional single-pass EDFA, the system without feedback exhibits a fairly flat gain spectral in the detuning range from -12 nm to 5 nm. At this pump power, the signal gain is ≤ 26 dB with the maximum signal gain of 26 dB achieved at $\Delta\lambda \approx 0$ nm. A higher gain is achieved for the regenerative-feedback scheme in the wavelength range of study. However, the gain spectral is not flat due to the resonant amplification characteristics of the regenerative-feedback amplifier. The highest gain is achievable near the resonance. In this range, the signal gain is 6 dB higher than the case without feedback. At the negative detuning of $\Delta\lambda_- \leq$ 14 nm and the positive detuning of $\Delta\lambda_+ \geq 10$ nm, the signal gains tend to be identical since the resonant amplification is no longer preserved for the large detuning.

In Fig. 6.26, noise figure as a function of $\Delta\lambda$ with a small $P_{in} = -30$ dBm is illustrated. A lower noise figure is achieved by the regenerative-feedback scheme for $\Delta\lambda_- < 5$ nm as compared to the system without feedback. However, the data scattering is relatively large for the former especially in the wavelength regime around the resonance under this near-threshold condition. A smaller data scattering is achievable for regenerative-feedback scheme if a lower power, for example, 23.8 mW, is used as shown in the inset.

The saturation input signal, P_{in}^{sat}, is studied as a function of signal detuning, $\Delta\lambda$, as denoted in Fig. 6.27. The P_{in}^{sat} is determined by 3-dB gain compression from the plot of signal gain versus input signal, P_{in} as shown in Fig. 6.22. The pump power was P_p = 29.4 mW. The saturation behavior of the regenerative-feedback amplifier has been described in Section 6.4.1.2. At the resonance, a small P_{in} = –32.6 dBm is sufficient to saturate the regenerative amplifier system due to the strong resonant amplification. Without the feedback, the P_{in}^{sat} increases markedly at the small detuning. The discrepancy of P_{in}^{sat} between both schemes diminish at the large detuning since the resonant amplification characteristics of the regenerative amplifier is no longer preserved.

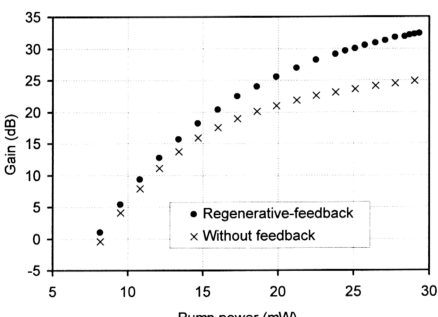

Fig. 6.20 *Signal gain as a function of the below threshold pump power.*

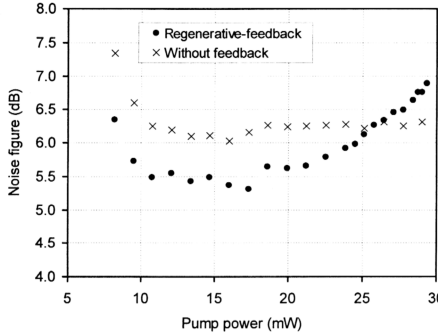
Regenerative-feedback
Without feedback
Noise figure (dB)
Pump power (mW)
8.0
7.5
7.0
6.5
6.0
5.5
5.0
4.5
4.0
5
10
15
20
25
30

(a)

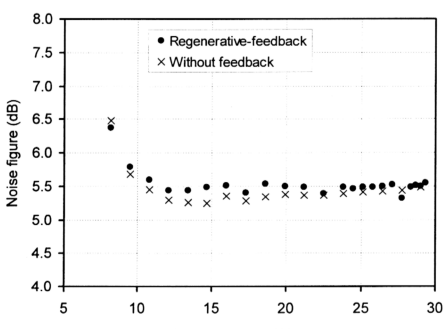
Regenerative-feedback
Without feedback
Noise figure (dB)
Pump power (mW)
8.0
7.5
7.0
6.5
6.0
5.5
5.0
4.5
4.0
5
10
15
20
25
30

(b)

(continue...)

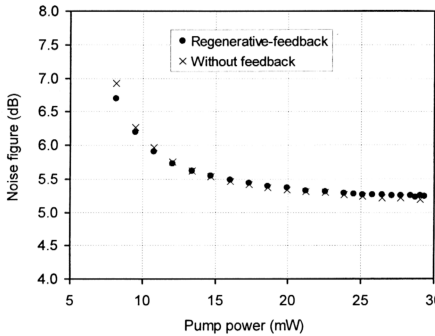

(c)

Fig. 6.21 *Pump power dependence of the noise figure for (a). P_{in} = -40 dBm (b). P_{in} = -30 dBm and (c). P_{in} = -10 dBm.*

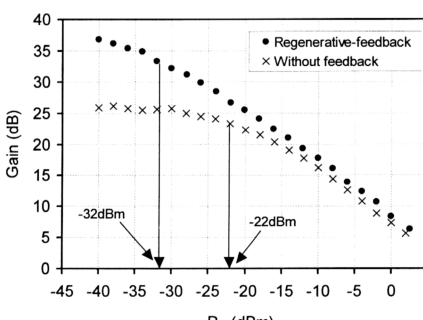

Fig. 6.22 *Signal gain as a function of input signal power is compared between the schemes with the pump power of 29.4 mW.*

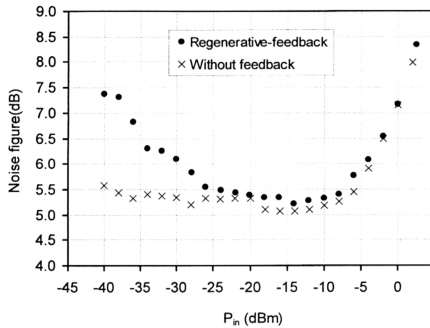

Fig. 6.23 *Noise figure versus input signal power at the pump power of 29.4 mW.*

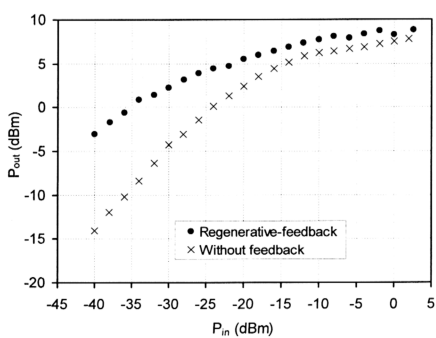

Fig. 6.24 *Amplified signal output power as a function of input signal power.*

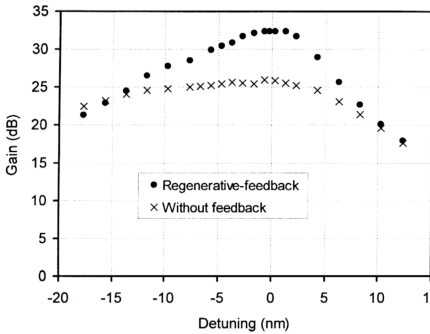

Fig. 6.25 *Signal gain versus signal detuning at the P_p = 29.4 mW. The input signal was fixed at P_{in} = -30 dBm and detuned from the potential lasing mode of 1557.7 nm.*

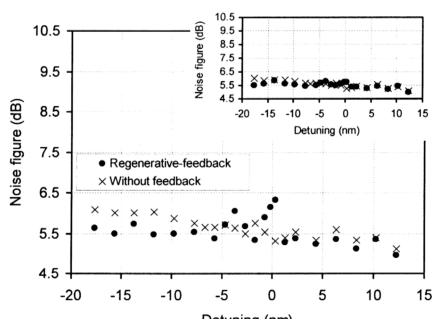

Fig. 6.26 *Noise figure versus signal detuning at the P_p = 29.4 mW. The input signal was fixed at P_{in} = -30 dBm and detuned from the potential lasing mode of 1557.7 nm. Inset shows a smaller data scattering with a lower power of 23.8 mW.*

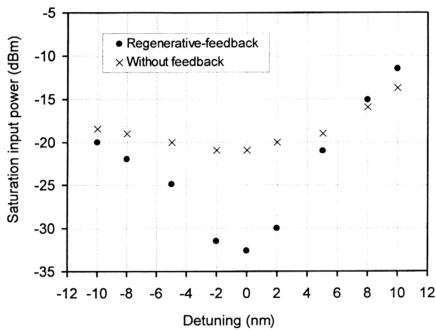

Fig. 6.27 *Saturation input signal as a function of signal detuning.*

6.4.2 Operation Above Threshold

6.4.2.1 Amplifier Performance

In this section, the regenerative EDFA system is studied above the oscillation threshold. With the small external signal injected to the system, there would be two modes, including the laser mode, existing simultaneously in the cavity. Figs. 6.28(a) and (b) show the output spectrum with the existence of two modes: one is the input signal at λ_{sig} = 1550 nm and the other one is the oscillating laser mode at λ_{laser} = 1557.7 nm. With the input signal of P_{in} = -30 dBm, the regenerative amplifier system starts to oscillate at the pump power of P_p = 29.4 mW. Figs. 6.28(a) and (b) illustrates the output spectrum for the system pump at 1.5 times and twice above the oscillation threshold, respectively. Note that the ASE level basically remains unchanged for different pump powers above the oscillation threshold.

With the signal injected at λ_{sig} = 1550 nm, the gain is investigated as a function of the pump power, P_p as denoted in Fig. 6.29. For the small signals of P_{in} = -30 dBm and –40 dBm, the signal gain increases progressively for ≤ 30 mW. After P_p ≥ 30 mW, the gain for both small input signals becomes independent of the P_p, indicating the occurrence of gain-clamping effect. The clamped-gains for both P_{in} are identical, i.e., 30 dB. With a higher P_{in} = -10 dBm, gain quenching by the strong input signal causes the regenerative amplifier to operate below the oscillation threshold. In this case, there is only the injected signal existing in the cavity. As a result, the gain-clamping effect is no longer observed. The signal gain increases with the pump power similar to the case of the conventional single-pass EDFA.

Fig. 6.30 denotes the dependence of the noise figure on the pump power, P_p. It differs from the below threshold case as shown in Fig. 6.21(a) where the P_{in} = -40 dBm exhibits an increase in the high pump region. Above the oscillation threshold, the existence of the oscillating laser in the anti-clockwise direction is able to effectively suppress the backward ASE. Without the strong backward ASE, the inversion level at the EDF input end is dependent on the pump power. In consequence, the noise figure decrease with the pump power. The lowest noise figure (4.5 dB) is achieved at the maximum available pump power P_p = 134.5 mW for P_{in} = -40 dBm. Although a much higher noise figure is expected for P_{in} = -10 dBm, further suppression of the backward ASE by this moderately strong input signal maintains the inversion at high level at the EDF input end. Therefore, the noise figure as low as 5 dB is achievable at P_p = 134.5 mW.

Amplified output power, P_{out} versus input signal power, P_{in} is depicted in Fig. 6.31. A higher P_{out} is obtained for the higher P_{in}. With the small signal P_{in} = -40 dBm, no further amplification is observed after the onset of the oscillation threshold due to

the gain-clamping effect. Instead of providing the gain to the input signal, the addition pump power fed into the metastable level goes into the oscillating laser mode [9]. Without the gain-clamping effect when the input signal is higher (P_{in} = -10 dBm), the input signal can be further amplified with a higher P_p.

Fig. 6.32 shows the power conversion efficiency, PCE, for different P_{in} as a function of the pump power. As described in Chapter 4, PCE can be used to determine the oscillation threshold of the EDFA system with the small input signals. From the figure, the oscillation threshold, determined by the maximum PCE, is found to be 28.4 mW and 29.4 mW, respectively for P_{in} = -40 dBm and –30 dBm. Due to the gain quenching effect, a higher pump power is required to achieve the oscillation threshold for P_{in} = -30 dBm as compared to the case of P_{in} = -40 dBm. Note that the amplifier system is operating below oscillation threshold when higher input signal P_{in} = -10 dBm is injected to the system. Therefore, the PCE in this case increases continuously with the pump power without exhibiting a maximum PCE.

In Fig. 6.33 signal gain as a function of input signal power, P_{in}, is presented. As compared to the case below threshold (see Fig. 6.10), the regenerative amplifier system operating above threshold exhibits a higher dynamic range, or a higher saturation input power, P_{in}^{sat}. Due to the gain-clamping effect, both pump powers of P_p = 44.0 mW and 58.7 mW achieve the same small-signal gain of ~29 dB with the maximum gain deviation of 1.1 dB. With the P_p = 44 mW, the saturation input power is P_{in}^{sat} = -15 dBm. By increasing the pump power by 1.25 dB. P_{in}^{sat} is increased by 2.5 dB since a higher pump results in a stronger gain-clamping effect.

Fig. 6.34 denotes the noise figure versus input signal power, P_{in}. A dip is observed at $P_{in} \approx$ -15 dBm due to the effectiveness of the backward ASE suppression

at this input level. There are not much differences in the noise figure between both pump powers except in the heavily saturated regime. Since the strong saturating input signal is able to effectively suppress the backward ASE, the inversion level at the EDF input end is dependent on the pump power under this strong injection condition. Therefore, the amplifier system achieves a lower noise figure for the higher pump power of P_p = 58.7 mW.

The amplified output signal power, P_{out}, is plotted as a function of P_{in} as shown in Fig. 6.35. In the unsaturated regimes the output powers are identical for both pump powers P_p = 44 mW and 58.7 mW. A striking feature is that after P_{in} > -20 dBm, P_{out} starts to depart from each other. This is attributed to the elimination in the gain-clamping effect in the amplifier system. As shown in Fig. 6.36, there is only the injected mode existing in the cavity for both pump power of 44 mW (Fig. 6.36(a)) and 58.7 mW with P_{in} = -18.5 dBm (Fig. 6.36(b)). The oscillating laser mode at the wavelength of 1557.7 nm as shown in Fig. 6.28 is suppressed to be below oscillation threshold due to the gain quenching induced by the saturated signal. The regenerative amplifier is now oscillating at the wavelength of the injected signal. This phenomenon is referred to as injection locking where the cavity is dominated by the external signal. A detailed study will be presented in Sec. 6.5. The system thus behaves like a conventional single-pass EDFA and the P_{out} becomes pump power dependent.

Fig. 6.37 shows the signal gain as a function of signal detuning. The pump power was fixed at P_p = 58.7 mW. The resonant amplification is only preserved for small signal of P_{in} = -30 dBm with the maximum gain of 38.9 dB achieved at the resonance. Strong saturation is observed for the input signal of P_{in} = -10 dBm and 0 dBm. In this case, the regenerative amplifier is operating below the oscillation threshold, leaving only the injected signal circulating in the cavity. Under this

condition, a flat gain is achievable over the amplification bandwidth with the signal gain reduces to 21 dB and 11 dB for P_{in} = -10 dBm and 0 dBm, respectively.

The noise figure as a function of signal detuning is illustrated in Fig. 6.38. With the saturating signal P_{in} = 0 dBm, saturation at the EDF input end causes the noise figure to be > 6 dB over the amplification bandwidth. A lower noise figure of ~ 5 dB is achievable for P_{in} = -10 dBm since the backward ASE is effectively suppressed and saturation effect is relatively small. Note that the data scattering is large in the case of P_{in} = -30 dBm. As referred to the Eq. (3.2), the noise figure is signal gain dependent. Variation in the signal gain will eventually change the noise figure. With this small input signal, the gain deviation is relatively large as compared to the case of higher P_{in}. A plausible explanation for such a variation is interference between the input signal and the circulating input signal. This would be described in detail in Sec. 6.4.2.3.

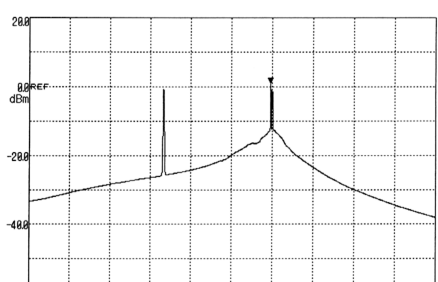

(a) *(continue...)*

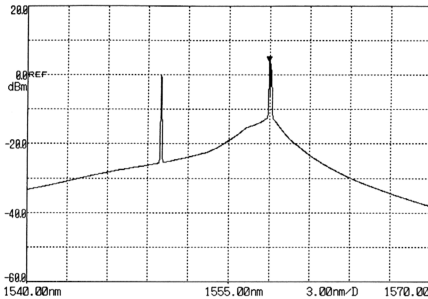

(b)

Fig. 6.28 *Output spectrum with input signal at λ_{sig} = 1550 nm and P_{in} = -30 dBm. (a) Pumped at 1.5 times above the oscillation threshold and (b) Pumped at twice above the oscillation threshold.*

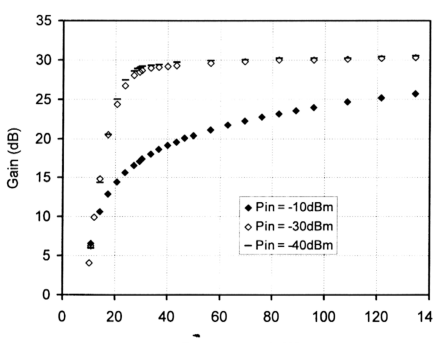

Fig. 6.29 *Signal gain as a function of pump power for different input signal powers.*

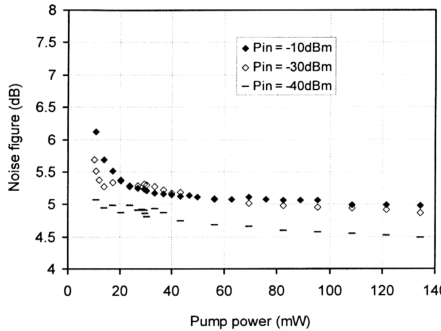

Fig. 6.30 *Dependence of the noise figure on the pump power.*

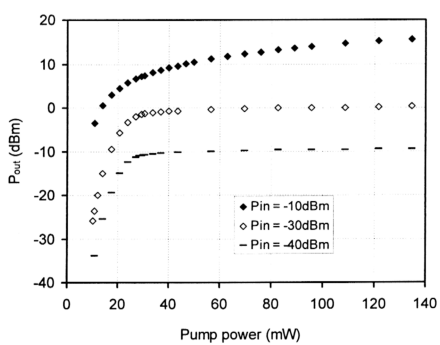

Fig. 6.31 *Amplified output power versus input signal power.*

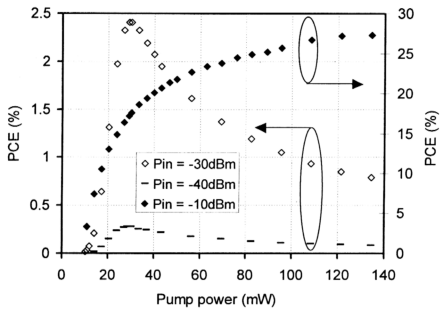

Fig. 6.32 *Power conversion efficiency for different input signal powers as a function of the pump power.*

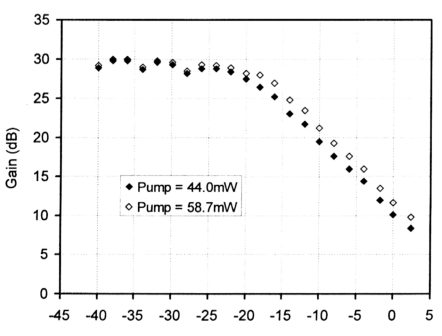

Fig. 6.33 *Signal gain as a function of input signal power*

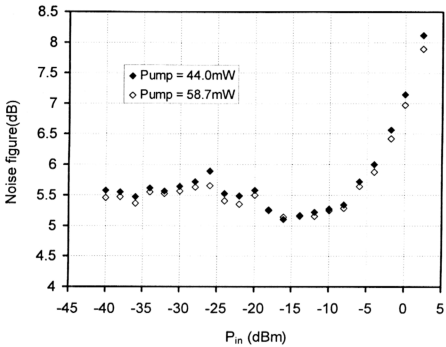

Fig. 6.34 *Noise figure versus input signal power.*

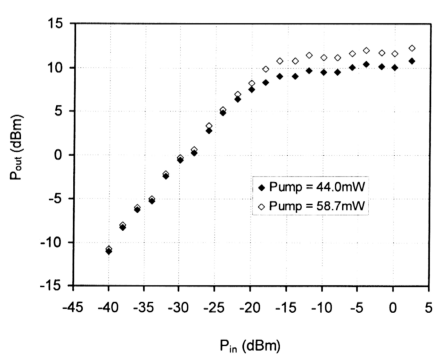

Fig. 6.35 *Amplified output signal power as a function of input signal power.*

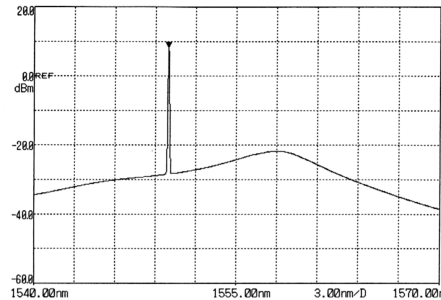

(a)

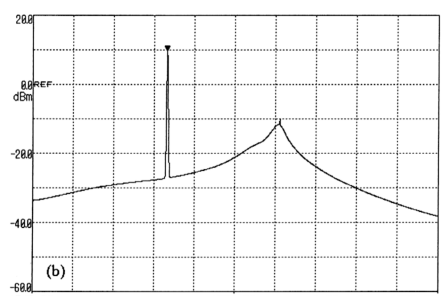

(b)

Fig. 6.36 *Output spectrum with the input signal power of –18.5 dBm. There is only the injected mode existing in the cavity for both pump power of (a) P_p = 44 mW and (b) P_p = 58.7 mW.*

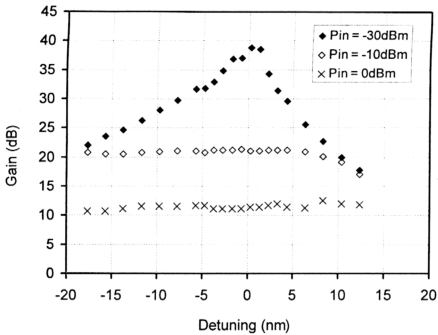

Fig. 6.37 *Signal gain as a function of signal detuning. The pump power was fixed at P_p = 58.7 mW.*

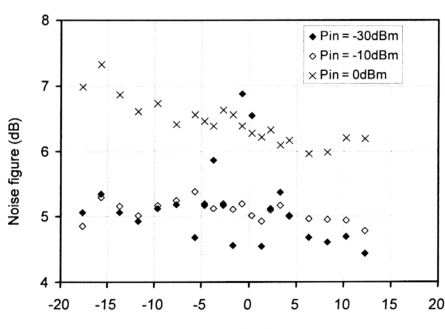

Fig. 6.38 *Noise figure as a function of signal detuning. The pump power was fixed at P_p = 58.7 mW.*

6.4.2.2 Comparison with the System Without Feedback

In this section, comparison is done between the EDFA with regenerative-feedback and that without feedback. With the signal injected at λ_{sig} = 1550 nm, the signal gains for both schemes are compared as a function of the pump power as depicted in Fig. 6.39. Fig. 6.39(a) shows the data with P_{in} = -30 dBm. Due to the gain-clamping effect in the regenerative-feedback scheme, the signal gain is independent of the pump power at the high pump. The maximum gain achieved in this case is 30 dB. Without the feedback, the signal gain continuously increases and exceeds that of the former scheme after P_p > 60 mW. The maximum gain is 2.3 dB higher at the maximum available pump power P_p = 134.5 mW. The inset shows the PCE for both schemes. In the regenerative-feedback scheme, the oscillation threshold is determined to be 29.4 mW after which the PCE starts to decrease. The description for this tendency has been given in Chapter 4. Without the feedback, the PCE increases at the low pump powers and starts to saturate at ~1.6 % after P_p = 80 mW. The efficiency of the power conversion in this scheme is limited by the ASE-induced saturation at the high pump powers. The PCE exceeds that of the regenerative-feedback scheme after P_p > 60 mW. Note that the plot differs from that illustrated in Fig. 4.14 and Fig. 4.28 in Chapter 4 at the low pump power in the sense that the regenerative-feedback scheme exhibits a higher PCE around the oscillation threshold. Regenerative-feedback in this case allows a higher regenerative amplification and thus a higher efficiency of the power conversion. With the saturating signal of P_{in} = -10 dBm as shown in Fig. 6. 39(b), the gain-clamping effect diminishes and the signal gain becomes dependent of pump power. The regenerative amplification system in this case is similar to the system without feedback. However, the scheme still achieves a gain ~1 dB higher due

to the regenerative amplification over the whole pumping range. The maximum achievable gain is 25.7 dB when the pump power is the maximum at 134.5 mW.

Figs. 6.40(a) and (b) show the noise figure versus the pump power P_p with the signal injected at λ_{sig} = 1550 nm. In the case of P_{in} = -30 dBm (Fig. 6.40(a)), both schemes exhibits a behavior opposite to each other. Without the feedback, the noise figure increases with the pump power. Existence of the backward ASE in the EDF input portion in this co-pumping scheme saturates the active medium in this end, resulting in the degradation in the noise figure. The noise figure increases linearly with the pump power with the slope of 4.4×10^{-3} dB/mW. By introducing the feedback in the direction of the input signal, the backward ASE can be effectively suppressed by the oscillating laser, depending on the strength of the laser mode. In consequence, the noise figure starts to decrease after the oscillation threshold at P_p = 29.4 mW since the inversion level at the EDF input end increases with the pump power under this condition. With the saturating signal of P_{in} = -10 dBm (see Fig. 6.40(b)), the backward ASE will be suppressed. As a result, a lower noise figure (< 5.5 dB) is obtained at the high pump regime as compared to previous case (P_{in} = -30 dBm) where the noise figure > 6 dB. However, the improvement of noise figure by the backward ASE suppression is balanced by the signal-induced saturation. Consequently, the noise figure becomes constant after P_p > 50 mW. Existence of the oscillating laser in the case of the regenerative-feedback scheme causes the mechanism of the backward ASE suppression dominating the process. Therefore, the noise figure is not only lower, as compared to that of the system without feedbacks but also decreases with the pump power. If the input coupling loss of 1.53 dB is excluded, intrinsic noise figure as low as 3.5 dB is achieved at the maximum pump

power of P_p = 134.5 mW. This indicates that near-complete inversion is achieved at the EDF input end.

Signal gain as a function of input signal power, P_{in} at the pump power P_p = 58.7 mW, twice above the oscillation threshold is denoted in Fig. 6. 41. The signal wavelength was fixed at λ_{sig} = 1550 nm. As referred to Fig. 6.38, this pump power is corresponding to the regime where the signal gains for both schemes are identical. Therefore, both schemes exhibit the same small-signal gain of ~29.5 dB in the unsaturated regime. With the existence of the gain-clamping effect in the regenerative amplifier system, a larger dynamic range is achieved. The saturation input power, by 3-dB gain compression, is determined to be P_{in}^{sat} = –15 dBm. The P_{in}^{sat} is 5 dB lower for the system without feedback. Operating below the oscillation threshold, the P_{in}^{sat} was found to be much lower as presented in Fig. 6.22 due to the absence of the gain-clamping effect.

Fig. 6. 42 shows the dependence of the noise figure on the P_{in} at the pump power twice above the oscillation threshold with the input signal wavelength fixed at λ_{sig} = 1550 nm. In the unsaturated regime, the regenerative-feedback scheme exhibits a noise figure ~0.5 dB lower than that obtained by the system without feedback. In this regime, the unsaturated signal is not able to suppress the backward ASE effectively, resulting in a relatively high noise figure for both cases. However, existence of the oscillating laser at the given pump power plays a role of backward ASE suppression, thus exhibiting a lower noise figure in the unsaturated regime. Above the input signal P_{in} > -20 dBm, the backward ASE suppression is the most efficient when $P_{in} \approx$ -12 dBm after which the signal-induced saturation starts to come

into effect. This process dominates the system in the heavily saturated regime i.e. at P_{in} = 0 dBm where the strong saturation takes place.

Fig. 6. 43 shows the amplified output power P_{out} of regenerative-feedback scheme as compared to that of the system without feedback. With the pump power twice above the oscillation threshold, the input signal was injected at the wavelength of λ_{sig} = 1550 nm. In the unsaturated regime, linear amplification is possible. There is a sudden change in the slope for the regenerative-feedback at P_{in}^{sat} = -16 dBm, corresponding to the situation where the oscillating laser mode starts to be locked to the injected signal. Above P_{in} > -16 dBm, P_{out} is independent of P_{in} and P_{out} as high as 11.7 dB is obtained. Without the feedback, the slope change gradually.

Figs. 6.44(a) and (b) denotes the dependence of signal gain on the signal detuning at the pump power twice above the oscillation threshold. With the unsaturated input signal fixed at P_{in} = -30 dBm as shown in Fig. 44(a), the superiority of the regenerative amplifier over the system without feedback is that resonant amplification exhibits a high gain in the signal detuning ranging from –8 nm to 5.3 nm. Resonant gain as high as 38.9 dB is achieved as compared to the system without feedback which achieves the gain by 8.7 dB lower. As shown in the inset, the output spectrum without input signal for the regenerative-feedback scheme (thick line) is higher than the case without feedback (thin line) from the wavelength of 1550 nm to 1565 nm. The peak at the wavelength of 1557.7 nm for the regenerative amplifier is the oscillating laser mode, with the saturating signal of P_{in} = -10 dBm, saturation effect in both systems causes the signal gain to be identical as shown in Fig. 6.44(b). A flatter gain spectral is achieved for both schemes. However, the signal gains degraded to < 22 dB.

Noise figure versus signal detuning at the P_p = 58.7 mW is illustrated in Figs. 6.45(a) and (b). In the case of P_{in} = -30 dBm as shown in Fig. 6.45(a), the strong backward ASE degrades the noise figure performance in the system without feedback. With the regenerative-feedback, this backward ASE is suppressed by the oscillating laser in the anti-clockwise direction, thus a lower noise figure (< 5.5 dB) is achievable. However, the data scattering is large due to the interference effect, as will be described in next section. The interference effect can be greatly minimized if the saturating signal with P_{in} = -10 dBm is applied. Fig. 6.45(b) shows that both systems achieve the noise figure very close to each other. With this P_{in}, injection-locking takes place and gain-clamping effect diminishes. The noise figures for both systems are still low since the backward ASE is effectively suppressed at this P_{in}, corresponding to the dip in the noise figure as shown in Fig. 6.42.

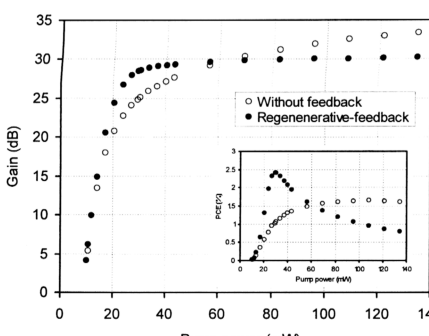

(a)

(continue...)

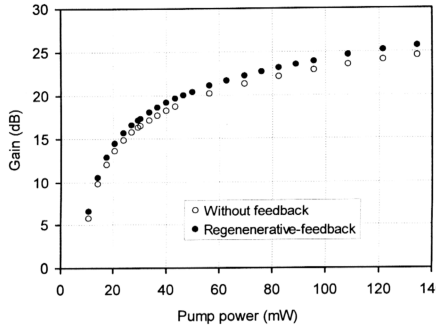

(b)

Fig. 6.39 *Signal gain for both systems with regenerative-feedback and without feedback as a function of the pump power. (a) P_{in} = -30 dBm. Inset shows the power conversion efficiency. (b) P_{in} = -10 dBm.*

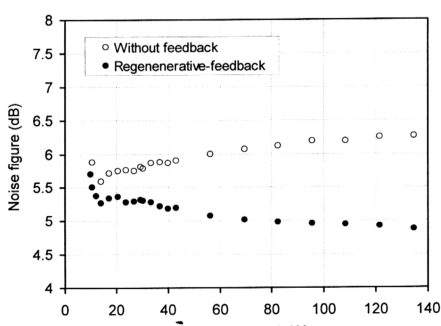

(a)

(continue...)

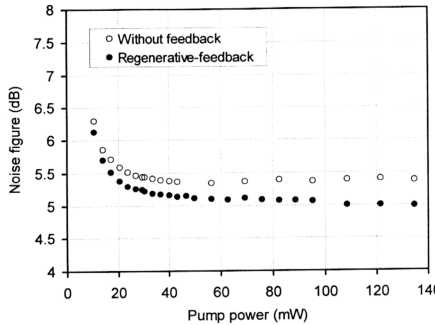

(b)

Fig. 6.40 *Noise figure for both systems with regenerative-feedback and without feedback as a function of the pump power. (a) P_{in} = -30 dBm. (b) P_{in} = -10 dBm.*

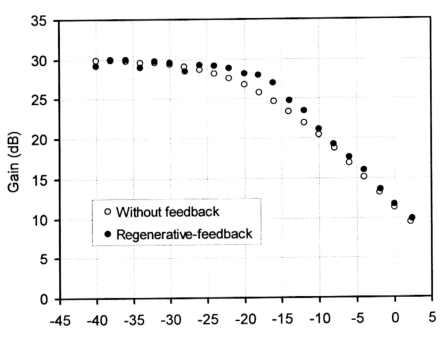

Fig. 6. 41 *Signal gain as a function of input signal power at P_p = 58.7 mW, twice above the oscillation threshold.*

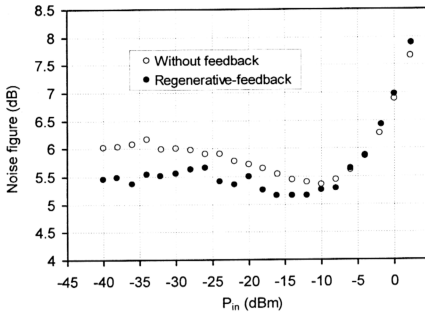

Fig. 6. 42 *Noise figure as a function of input signal power at $P_p = 58.7$ mW, twice above the oscillation threshold.*

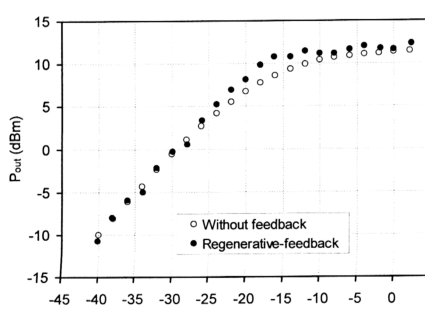

Fig. 6.43 *Amplified output signal power versus input signal power.*

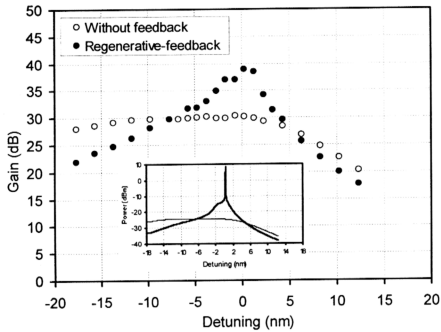

(a)

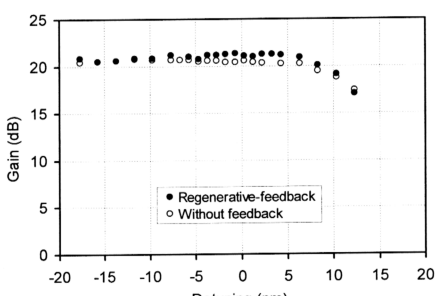

(b)

Figs. 6.44 *Dependence of signal gain on the signal detuning at the pump power twice above the oscillation threshold. (a) P_{in} = -30 dBm. Inset shows output spectrum without input signal. (b) P_{in} = -10 dBm*

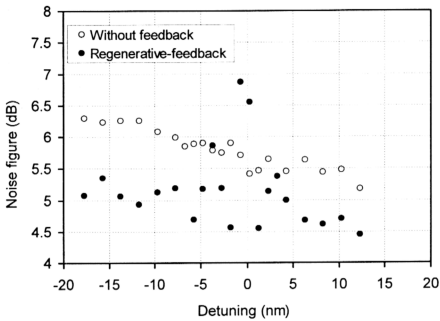

(a)

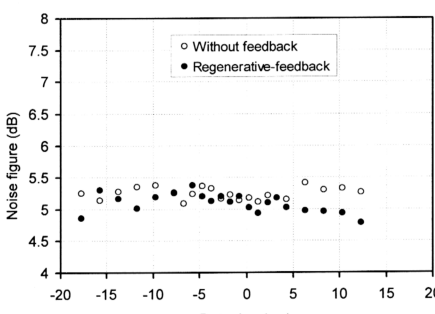

(b)

Figs. 6.45 *Dependence of noise figure on the signal detuning at the pump power twice above the oscillation threshold. (a) P_{in} = -30 dBm. (b) P_{in} = -10 dBm.*

6.4.2.3 Comparison with Co-feedback Scheme

In this section, the regenerative-feedback EDFA is compared with the co-feedback EDFA above the oscillation threshold. In both systems, the oscillating lasers are oscillating in the direction of the input signal. The difference between both systems is that the wavelength selective element, or tunable bandpass filter (TBF) in our case, is removed from the ring cavity for the regenerative-feedback scheme. Without the wavelength selective element, the injected signal experiences regenerative-feedback and thus regenerative amplification through circulation in the cavity. On the other hand, the injected signal experiences only a single-pass amplification in the co-feedback system.

Fig. 6.46 shows the forward ASE spectrum without the input signal for the regenerative-feedback scheme (thick line) and the co-feedback scheme (thin line) at the pump power of 43.4 mW with the resolution set at 0.02 nm. Without the bandpass filter, the regenerative-feedback system exhibits a higher output power at the region around the oscillating mode of 1558 nm. Other than the selected mode at 1558 nm, the output spectrum for the co-feedback system is purely from the forward single-pass ASE. In the regenerative-feedback configuration, a significant suppression of the output power was observed for the wavelength below 1530 nm due to the absorption of the photons in this wavelength regime. This is balanced by the energy needed to provide amplification of the input signal at the longer wavelengths. Therefore, a higher inversion level at the wavelength range from 1540 nm to 1565 nm is achieved through the thermalization process among the sublevels of the metastable level according to Boltzmann distribution [10] .

Since the feedback mechanism is introduced in both systems, gain-clamping effect is observed after the onset of the laser oscillation. Fig. 6.47 shows that the

signal gains are independent of the pump power above the laser threshold for the input signal power P_{in} = -31.2 dBm. Signal gain as high as 30 dB is achieved in the regenerative-feedback scheme. In this case the system starts to lase at the pump power of P_p = 29.4 mW. For the co-feedback scheme, a lower pump power (23.8 mW) is required to achieve the laser oscillation. Therefore, the population is fixed at a lower inversion level. This results in a lower clamped-gain of 23.3 dB after the onset of laser oscillation. Such a lower inversion also causes a higher noise figure in this system as compared to that of the regenerative-feedback system. Note that the signal gains from the simulation for both co-feedback and regenerative-feedback are higher than that obtained experimentally with the regenerative-feedback scheme achieve a larger deviation.

Fig. 6.48 shows that the regenerative-feedback scheme achieves a noise figure ~1 dB lower than that of the co-feedback scheme at the maximum pump power of 134.5 mW. In the regenerative-feedback scheme, a higher average inversion level is achieved at the sublevels corresponding to the wavelength above 1540 nm. Besides the backward ASE suppression by the oscillating laser mode at 1558 nm, the higher ASE floor level in the wavelength range from 1545 nm to 1565 nm in the regenerative-feedback scheme also plays a role in further suppression of the backward ASE at the EDF input end. Fig. 6.49 shows the backward ASE output from the 1 % port of the coupler C_3 in the anti-clockwise direction for both feedback schemes. The thick line represents the regenerative-feedback scheme whereas the thin line is for the co-feedback scheme. It is evident that the regenerative-feedback scheme exhibits a lower backward ASE. Therefore, a higher inversion level is expected at the EDF input end. Excluding the input coupling loss of 1.53 dB, the noise figure as low as 3.2 dB is achieved for the system with the regenerative-feedback at the maximum pump,

indicating a nearly complete inversion at the EDF input end. A striking feature is that the simulation result is higher for the regenerative-feedback scheme. Such a deviation might due to the assumption in the model that the components losses are wavelength independent. However, the wavelength dependency of the component losses become significant when the tunable bandpass filter is omitted.

Fig. 6.50 shows the dependence of the signal gain on input signal power, P_{in} for a fixed pump power of P_p = 89 mW. For the regenerative-feedback scheme, gain-clamping effect is not as strong as that of the co-feedback scheme. A larger dynamics range is obtained for the co-feedback scheme where it starts to saturate at P_{in}^{sat} = -7 dBm with the small-signal gain of 23.3 dB. In the regenerative-feedback scheme, the circulating signal, which experiences regenerative amplification and thus a higher gain, tends to saturate the gain medium even with a small signal power. In this case, the P_{in}^{sat} is 7 dB smaller than that of the co-feedback scheme. Note that a good agreement between the simulation results and experimental data is only achieved in the saturation regime.

Fig. 6.51 shows the noise figure as a function of input signal power, P_{in}. Note that the dip effect is not observed experimentally for either scheme. At the pump power of P_p = 89 mW, the backward ASE is relatively low and the oscillating laser is high enough to suppress it. Therefore, no further suppression of the backward ASE is possible even in the moderately saturated regime. Noise figure as low as 4.8 dB is achievable in the regenerative-feedback scheme in the unsaturated regime. For the co-feedback scheme, the noise figure is ~1 dB higher. The discrepancy of the data might also arise from different characterization methods: TDE method for co-feedback scheme and Interpolation for regenerative-feedback scheme. It s worth noting that the

dip effect is obvious in the simulation for the co-feedback scheme. In the saturation regime, however, the discrepancy between the simulation and the experiment for both schemes is relatively large.

Excess pump power is taken as a function of input signal power, P_{in} as shown in Fig. 6.52. Due to a higher population at metastable (or smaller ground state population) for the small signals, the regenerative-feedback scheme exhibits a high excess power, or a lesser pump absorption. However, the excess power decreases with the P_{in} as a result of ion depopulation. A striking feature is that there is a minimum excess power after which the excess power starts to increase from the saturated input signal of P_{in} = -14 dBm. This reveals a reduction in the ground state population. In this moderately saturated regime, ground state absorption is found to be increasingly significant. In the case of co-feedback scheme, a stronger gain-clamping effect results in a constant excess power up to $P_{in} \approx$ -20 dBm. Increase in the excess power thereafter indicates that the ground state absorption process dominates the system. However, this process is balanced by the signal-induced depopulation at $P_{in} >$ -10 dBm.

In order to simulate the regenerative EDFA performance in the system level, bit-error-rate (BER) was evaluated using Tektronix ST2400 BER Tester (BERT) which produced a fixed data rate of 2.4 Gbit/s and a fixed signal wavelength of 1535.4 nm. A variable optical attenuator (VOA) and a TBF with a 3-dB bandwidth of 1.0 nm were inserted between the amplifier output and the receiver. The TBF was tuned to the wavelength of 1535.4 nm. With the output power controlled by a VOA at the maximum allowable BERT received power, the BER was obtained by varying the input signal power. The setup is shown in Fig. 6.53.

Figs. 6.54(a) and (b) show the BER as a function of input signal power, P_{in} for regenerative-feedback and co-feedback schemes, respectively. Two different pump powers of P_p = 23.8 mW and 69.4 mW are presented for comparison. The data shows that an error free performance is achieved with the saturating input power above P_{in} > -12 dBm for P_p = 23.8 mW and P_{in} > -4 dBm for P_p = 69.4 mW for regenerative-feedback scheme. For the co-feedback scheme, the performance is much better where the low BER can be obtained at a much lower P_{in}. Deterioration in the BER performance in the regenerative-feedback scheme can be attributed to the interference effect [11] that arises from such a configuration where the circulating input signal experiences phase change in each round-trip. With the same frequency but different phases, the interference between the input signal and the circulating input signal may take place. With the unsaturated input signals, the level of the circulating signal and the input signal are comparable since the small-circulating signal experiences high regenerative amplification. Therefore, the interference effect is significant, resulting in the degradation of the BER performance. With the saturating signal, the active medium is saturated and the level of the circulating signal is relatively low. Under this condition, the interference effect is minimized, giving a better BER performance. It has been shown that BER performance can be improved by forward error correction (FEC) method [12]. Note that such interference does not take place in the co-feedback scheme since the input signal experiences only a single-pass amplification.

It is worth noting in Fig. 6.54 that the BER performance for the regenerative-feedback scheme is markedly degraded when the pump increases from P_p = 23.8 mW to 69.4 mW as compared to the case of the co-feedback. The BER performance versus the pump power at P_{in} = -4 dBm is illustrated in Fig. 6.55. For the regenerative-feeback scheme as shown in Fig. 6.55(a), an error free performance can be achieved

at the $P_p < 60$ mW. The interference effect becomes increasingly significant with the higher pump powers due to the stronger amplification for both input signal and the circulating input signal. This is not the case for the co-feedback scheme where the BER performance is improved by increasing the pump power. At the low pump powers, the BER performance is degraded by signal absorption by the unpumped section of the EDF. An error free performance is eventually achieved above $P_p > 11$ mW.

Obviously, the BER performance is deteriorated significantly in the regenerative-feedback scheme. The data in Fig. 5.56 shows that the transmission performance is significantly degraded as the received power decreases. Data for back-to-back measurement (without EDFA) is also provided as a reference. Power penalty as high as 6 dB is observed for the input signal power of –8 dBm at 10^{-10} BER. A better BER performance can be achieved when the input power is increased to –4.3 dBm. Operating in such a saturation regime, the regenerative amplifier exhibits a potential application as a power amplifier. The data shows that, there is a limitation for such a configuration in the optical transmission system. However, this amplifier system has a potential application as a frequency-stabilized laser source, where the required frequency stability is provided by an external low power master laser. Thus, efficient power amplification can be realized. Such a potential application has been presented in the mainframe CO_2 laser system [1]. Operating above the threshold of self-oscillation, a stable power spectrum has been observed due to the suppression of the neighboring modes to the point that they are driven below threshold by the small external injection [13].

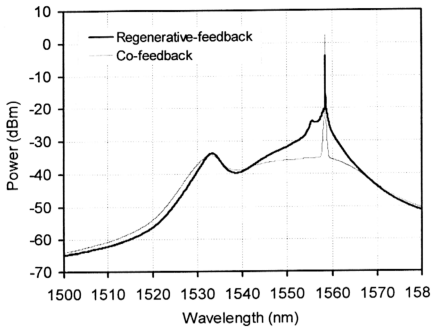

Fig. 6.46 *Forward ASE output without the input signal for regenerative-feedback scheme (thick line) and co-feedback scheme (thin line) at the pump power of 43.4 mW with the resolution set at 0.02 nm.*

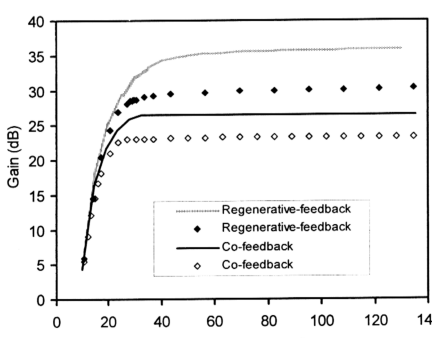

Fig. 6.47 *Dependence of signal gains on the pump power for P_{in} = -31.2 dBm. (Point signs: Measured results; lines: Simulation results).*

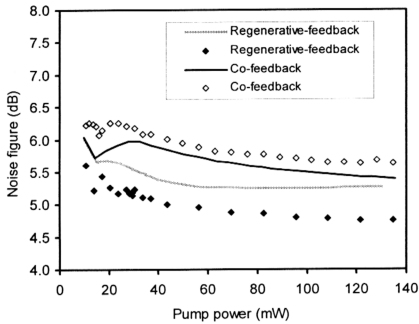

Fig. 6.48 *Dependence of noise figure on the pump P_{in} = -31.2 dBm. (Point signs: Measured results; lines: Simulation results).*

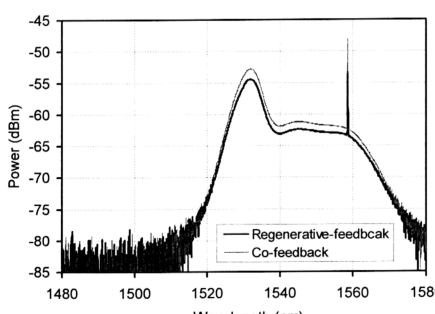

Fig. 6.49 *Backward ASE output from the 1 % port of the coupler C_3 in the anti-clockwise direction for both feedback schemes.*

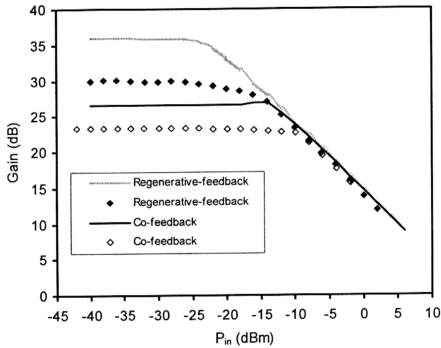

Fig. 6.50 *Dependence of the signal gain on input signal power for a fixed pump power P_P = 89 mW. (Point signs: Measured results; lines: Simulation results).*

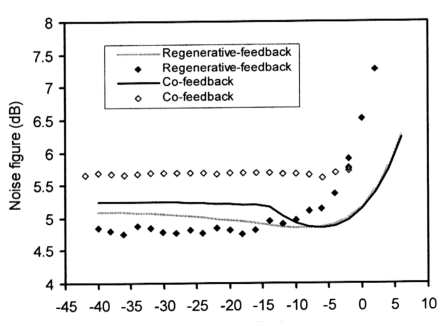

Fig. 6.51 *Noise figure as a function of input signal power at P_P = 89 mW. (Point signs: Measured results; lines: Simulation results).*

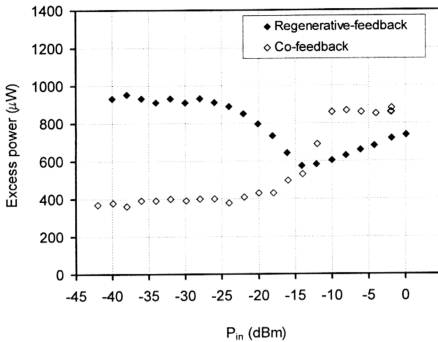

Fig. 6.52 *Excess pump power is taken as a function of input signal power.*

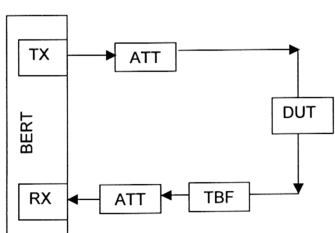

Fig. 6.53 *Experimental arrangement for BER measurement. (BERT: bit-error-rate tester; VOA: variable optical attenuator; TBF: tunable bandpass filter; DUT: EDFA).*

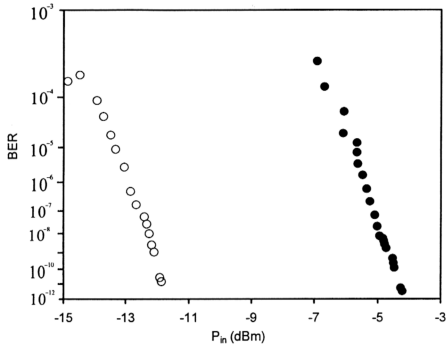

(a)

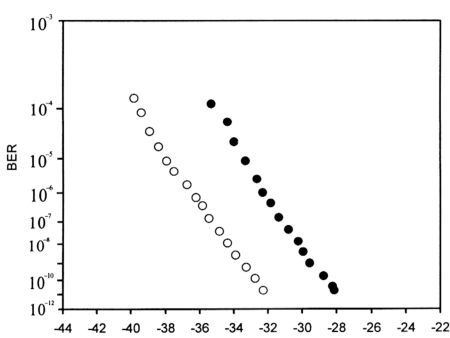

(b)

Fig. 6.54 *BER as a function of input signal power. (o: P_p= 23.8 mW; •: P_p = 69.4 mW) (a) regenerative-feedback and (b) co-feedback.*

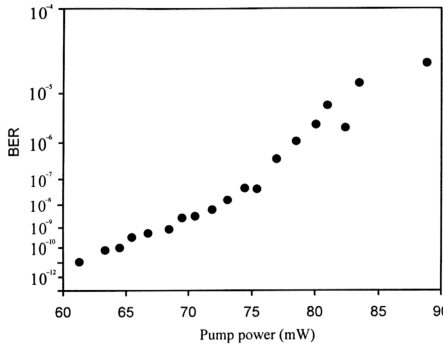

(a)

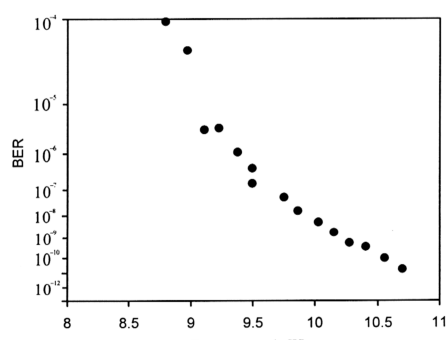

(b)

Fig. 5.55 *The BER performance versus the pump power with the input signal power of –4 dBm. (a) Regenerative-feedback and (b) Co-feedback.*

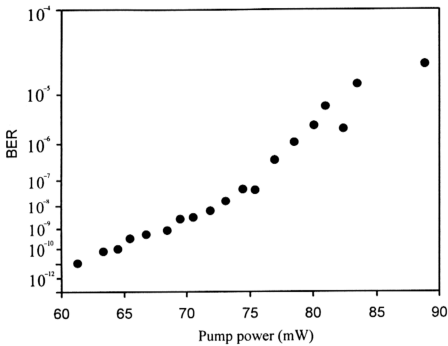

Fig. 5.55 *The BER performance versus the pump power with the input signal power of –4 dBm. (a) Regenerative-feedback and (b) Co-feedback.*

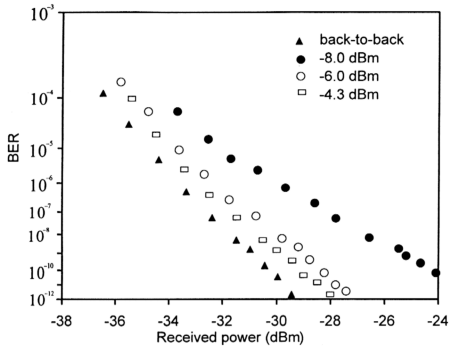

Fig. 5.56 *The BER performance for regenerative-feedback scheme versus received power with different input signal powers of –4.3 dBm, -6.0 dBm and –8.0 dBm. Back-to-back measurement is added as a reference.*

6.5 INJECTION-LOCKING

In this section, injection-locking phenomenon for the system operating above threshold is presented. Laser injection-locking was first demonstrated by Stover and Steiver [14], who directly injected the beam of one He-Ne laser into the resonator of a second He-Ne laser. In 1990, Jones and Urquhart [15] presented the first injection-locked erbium-doped fiber laser (EDFL) in a linear configuration. The injection-locking effects, besides having important practical application, provide an excellent illustration both of laser theory and of the fundamental principles of oscillator dynamics [9]. The theory of injection-locking that has been developed recently [16-19] predicts a few important phenomenon such as bistability, bifurcation and period-doubling route to chaos. Injection-locking phenomenon have been applied on a

various of laser system to stabilize the frequency [20], to lock the phase of a separate laser [21], to narrow the linewidth [22-24], to select the frequency of an injected laser [22], or to ensure single-mode operation [15].

Locking of a laser system, called the "slave laser", occurs when the free running oscillation frequency and the injected signal frequency from a "master laser" are close enough and when the injected intensity is high enough. Energy exchange between these components is expected to play an important role in the injection-locking phenomenon and a competition may occur between them [18]. Within the locking range, the self-oscillation of the locked laser is quenched, and only the amplified drive power of the injected laser appears. A theoretical description of the injection-locking based on Adler's Model is given in Appendix C.

Fig. 6.57 shows the amplified output power, P_{out}, as a function of input signal power, P_{in} for the signal detuning, $\Delta\lambda = \pm 5$ nm at the pump power $P_p = 58.7$ mW, twice above the oscillation threshold. The lasing wavelength in this system is 1558 nm. A lower output signal power for the positive detuning is attributed to asymmetrical in the ASE spectrum where the photons with the wavelengths larger than the oscillating laser mode experience a lower gain. Note that there is a sudden change in each slope. The point where the slope starts to change is corresponding to the injection-locking state. At this stage, the laser amplifier system starts to oscillate at the wavelength of the injected signal. Since the signal with the negative detuning experiences a higher gain, the P_{in} required to lock the laser is lower. Fig. 6.57 shows that the minimum P_{in} for injection-locking is –21 dBm for negative detuning and –16.5 dBm for positive detuning.

Figs. 6.58(a) and (b) show the output spectrum before and after the injection-locking, respectively, for the case where the injected signal is detuned by $\Delta\lambda = 5$ nm

from the oscillating laser mode at the wavelength λ_{laser} = 1558 nm. The pump power is twice above the threshold. With the input signal of P_{in} = -22 dBm (see Fig. 6.58(a)), there are two signals oscillating simultaneously in the cavity. Note that the injected signal is getting amplified and taking away portions of the gain from the oscillating laser. By increasing the signal power to P_{in} = -21 dBm, the gain of the oscillating laser is quenched and the system is dominated by the injected signal as shown in Fig. 6.58(b). The laser-amplifier system is thus operating the below threshold of self-oscillation.

Locking range as a function of P_{in} is illustrated in Fig. 6.59. It is defined as the maximum detuning for the injection-locking to occur. Inside the locking range, the amplifier system oscillates at the wavelength of the injected signal. Outside the locking range, both injected signal and oscillating laser modes present simultaneously in the cavity. From the figure, it is obvious that the locking range increases with the P_{in} for both cases of positive and negative detuning. The signal with negative detuning exhibits the locking range twice the positive detuning.

Due to the inhomogeneous broadening of the active medium, the erbium-doped fiber laser (EDFL) system suffers from the severe mode competition or frequency instability and thus power fluctuation. Injection-locking is a way to combat such a problem [25]. Fig. 6.60 shows that the fluctuated output spectral is improved by the external injection. Without the injection, a few modes oscillate successively as shown in Fig. 6.60(a). This results in fluctuation in the laser peak power. The stability can be improved by injecting an external signal, depending on the level of injection. Fig. 6.60(b) shows the output spectral with a small injection of –35.6 dBm. The spectral is still "spiky" with this injection level. With the injection level of –31.6 dBm, a more stable output spectral is observed as shown in Fig. 6.60(c). Most of the side

modes are suppressed to be below threshold. This is the mechanism of linewidth narrowing in an injection-locked laser system [13, 26]. All the side modes are completely locked to the injected signal when the injection level is high enough, for example, -17.6 dBm as shown in Fig. 6.60(d). Note that this injected signal is also getting amplified, giving a gain as high as 28.2 dB, or a stable output peak power of 10.6 dBm. Fig. 6.61 shows the output peak power from the slave laser system as a function of injection level at the pump power of 58.7 mW, twice above the oscillation threshold. The error bars show the amplitude of the peak power fluctuation. Obviously, the stability of the output power is improved by increasing the injection level. As shown in Fig. 6.61, the stability of the output peak power is basically achieved by the frequency stabilization through the injection-locking. Peak power > 10 dBm can be achieved with the injection level > -22.5 dBm.

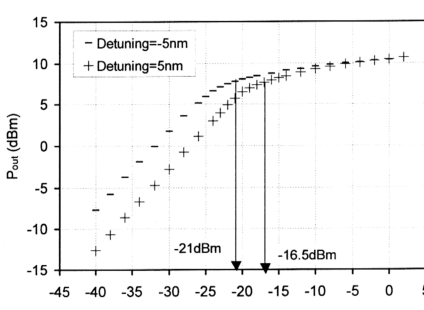

Fig. 6.57 *Amplified output power as a function of input signal power for the signal detuning of ± 5 nm at the pump power of 58.7 mW.*

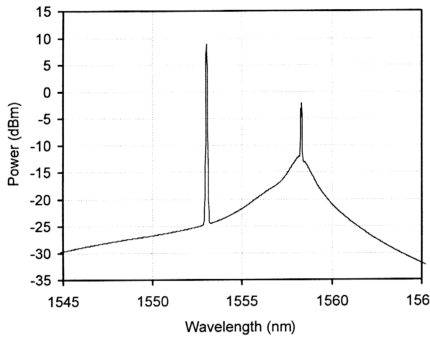

(a)

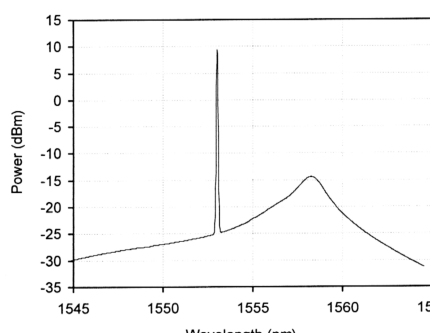

(b)

Fig. 6.58 *Output spectrum with external injection where the injected signal is detuned by 5 nm. (a) Before injection-locking with P_{in} = -22 dBm. (b) After injection-locking with P_{in} = -21 dBm.*

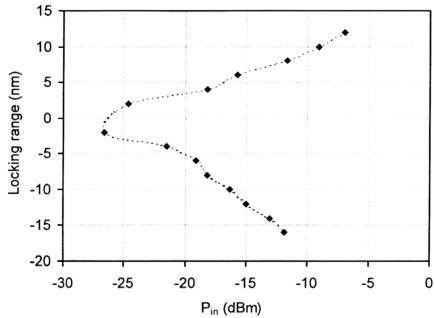

Fig. 6.59 *Locking range as a function of input signal power.*

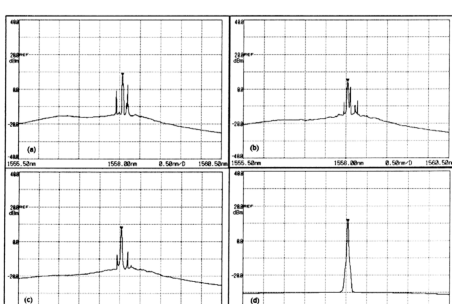

Fig. 6.60 *Fluctuated output spectral is improved by the external injection. (a). Without injection. (b). P_{in} = -35.6 dBm. (c). P_{in} = -31.6 dBm. (d). P_{in} = -17.7 dBm.*

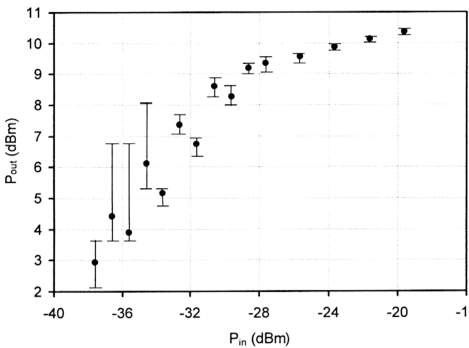

Fig. 6.61 *Amplified output signal power as a function of input signal power.*

6.6 REGENERATIVE AMPLIFIER SUBJECT TO EXTERNAL INJECTION

In this section, we present the results on the regenerative EDFA system subject to second injection at the pump power below threshold of self-oscillation. Performance of the amplifier system in terms of gain and noise figure have been improved under certain injection conditions. Although a similar phenomenon has been observed in the long-band (L-band) EDFA [27], we try to suggest a possible explanation of the mechanism for the phenomenon observed in this study.

Figs. 6.62(a) and (b) shows the ASE spectrum with and without probe signal, respectively, at the pump power of 10.8 mW, 0.4 times below the lasing threshold. The injection wavelength and injection power were 1530 nm and –11.8 dBm,

respectively. Since the pump power was low, the main peak at $\lambda \sim 1530$ nm progressively vanishes while the center of the ASE spectrum shifts towards longer wavelengths near $\lambda \sim 1558$ nm. The effect of progressive absorption at $\lambda = 1530$ nm is due to the fact that the overlap between absorption and emission cross sections is maximum at that wavelength [8]. Such pump-induced spectral changes are characteristic of three-level laser system in which the transition terminates to the ground level. Moreover, ground state absorption (GSA) is significant at the short wavelength centered at $\lambda = 1530$ nm. The thin line in Fig. 6.62(a) shows the ASE profile without external injection. With the external injection (thick line), the output spectrum increases for the whole spectrum ranging from 1400nm to > 1600 nm. In the single-pass long band (L–band) amplifier system [27], the same phenomenon has been observed where injection at the wavelength of 1550 nm enhanced the gain of L–band (1570 nm – 1610 nm). In order to investigate the performance improvement of the injected regenerative amplifier, a small probe signal with a fixed power of –30 dBm was injected at the resonant wavelength of 1558 nm where there is a potential laser mode. Onset of the lasing threshold will be observed at this mode if the pump power is above 29.4 mW. Fig. 6.62(b) shows the output spectrum with both injection signal and probe signal.

Gain enhancement of the probe signal as a function of the injection power is shown in Fig. 6.63. Three different pump powers of 17.3 mW, 23.8mW and 29.4 mW were studied. Fig. 6.63 shows that there is an optimum injection power for the maximum gain enhancement for each pump power. Pump power of 17.3 mW exhibits the highest gain enhancement of 2.5 dB at the injection power of –20 dBm. Above this injection power, gain degradation is observed due to the depopulation induced by the strong injection power. With the higher pump powers of 23.8 mW and 29.4 mW,

the maximum gain enhancement decreases to 0.7 dB and 0.4 dB, respectively. At the same time, the optimum injection powers also reduce to –24 dBm and –26 dBm, respectively. Note that there is no effect on the system at the small injection power of –40 dBm for different pump powers.

In Ref. [27], the authors attributed the gain enhancement to the secondary pump induced by the injected signal. If this is the fact, then increment in the output spectrum will only be observed for the wavelength longer than the injection wavelength due to the effect of phonons transition. However, Fig 6.62 and Ref. [27], show that the output spectrum also increase for the wavelengths shorter than the injection wavelength (<1530 nm in our case and <1550 nm in Ref [27]). In order to prove that the energy consumed by the amplification process for the entire bandwidth is not sourced by reductions in the forms of the pump power, excess pump power was studied as shown in Fig. 6.64. Instead of reduction, the excess pump powers exhibit an increment even with the injection power larger than the region where there is no gain enhancement. At the pump power of 17.3 mW, the maximum increment in the excess pump power, or in other words, minimum pump absorption, is at the injection power of –20 dBm corresponding to the maximum gain enhancement. In addition, it will be shown later that instead of absorption, the injected signal itself experiences amplification and the maximum amplification is obtained when the gain enhancement is maximum. Therefore, gain enhancement should not be purely attributed to the secondary pump source induced by the external injection. At this stage, we believe that a second mechanism comes into play. It has been demonstrated in the EDFA system that the injected signal is able to suppress the backward ASE in the under-pumped EDF [5-8]. This backward ASE depletes the population at the metastable level and degrades the amplifier performance. Suppression of backward ASE by the

injected signal then results in restoration of the population back to a higher inversion [7-8]. This reduces the ground state population and thus the pump power absorption. Consequently, we believe that performance improvement in this system and that in Ref. [27] can be attributed to the backward ASE suppression by the external injection.

The variation of the forward ASE profile has been shown in Fig. 6.62. For the backward ASE profile subject to external injection, the spectrum was taken from the 1% port of the coupler C_3 in the cavity (see Fig. 6.1) as shown in Fig. 6.65. The thin line in the figure shows the case without injection at the pump power of 10.8 mW. With an injected signal at the power of –10 dBm and at the wavelength of 1530 nm (thick line), a significant suppression of the backward ASE profile is observed.

Fig. 6.66 shows the noise figure penalty versus the injection power for different pump powers. Negative values indicate the improvement in the noise figure. With the optimum injection power of ~ –20 dBm, where the backward ASE is effectively suppressed, noise figures have been improved by 0.2 dB – 0.3 dB. Above the injection power of –12 dBm, noise figures start to degrade as a result of saturation induced by the strong external injection. The noise figure penalty increases exponentially with the injection power in this moderately saturated regime.

The dependence of the gain enhancement on the injection wavelength is depicted in Fig. 6.67. The injection power was fixed at –25 dBm for the different pump powers of 17.3 mW, 23.8 mW and 29.4 mW. For the low pump power of 17.3 mW, the gain enhancement can be obtained for the injection wavelengths ranging from 1520 to 1548 nm after which gain degradation starts to occur. Gain quenching by the injected signal takes place when the injection wavelength is close to the wavelength region around the probe signal. For the higher pump powers of 23.8 mW and 29.4 mW, gain degradation is observed with the injection wavelength beyond

1540 nm and 1538 nm, respectively. Within this tuning range, a maximum gain enhancement is achieved when the signal is injected at the wavelength of 1531 nm for the pump power of 17.3 mW and 1530 nm for both the pump powers of 23.8 mW and 29.4 mW. This indicates that backward ASE has been effectively suppressed with these injection wavelengths. Maximum gain enhancement of 2.2 dB is achieved with the pump power of 17.3 mW.

Noise figure penalty as a function of injection wavelength for different pump powers is presented in Fig. 6.68. It is obvious that noise figure penalty is high when the injected signal is detuned from the wavelength region around 1531 nm where the absorption and emission cross-section is the largest. The data points scattering is relatively large when the system is pumped at the power of 29.4 mW, just below the lasing threshold due to the increasingly significant of the interference effect as described in Sec. 6.4.2.3. The noise figure is improved only when the injected signal is tuned to the wavelengths around 1531 nm for the pump powers of 17.3 mW and 23.8 mW.

The output of the injected signal itself at a fixed wavelength of 1530 nm is studied as a function of the injection power. It was found that the injected signal experiences amplification for the given pump powers of 17.3 mW, 23.8 mW and 29.4 mW as shown in Fig. 6.69. A striking feature is that for the pump power of 17.3 mW, a maximum gain of 14.7 dB is achieved at the injection power of –22 dBm instead of the lower injection powers. A higher gain at this injection power can be attributed to the effectiveness of the backward ASE suppression which restores the population to a higher inversion level. This mechanism not only enhances the gain in the resonant regime, but also the entire Er^{3+} emission bandwidth, including the wavelength of the

injected signal itself. If the injected signal acts as a secondary pump source as claimed in Ref. [27], then it should experiences absorption instead of amplification.

The forward and backward ASE output spectrums were then taken for both co-pumping and counter-pumping schemes with the ring opened, in order to compare the mechanism of the gain enhancement effect for both pumping schemes. An optical isolator was spliced to each 5 % port of the coupler C_1 and C_2. Figs 6.70(a) and (b) show the co-and counter-pumping schemes, respectively. The output spectrums were taken from the 5% port. The systems were pumped at the power of 10.8 mW with the injection at the power of 2.3 dBm and the wavelength of 1530 nm. Note that *forward* and *backward* is the direction with respect to the input signal direction.

Fig. 6.71(a) and (b) show the forward and backward ASE spectrum, respectively, for the co-pumping scheme. The forward ASE was monitored from the 5% port of the coupler C_2 whereas the backward ASE was taken from the 5% port of the coupler C_1 as shown in Fig. 6.70(a). Therefore, the injected signal is not observed in the backward ASE spectrum. Considering the case without injection, the output spectrums for both forward and backward ASE are different from each other. In such a low inversion regime, GSA dominates at short wavelengths, resulting in vanishing of the main peak near 1530 nm. Traveling along the EDF with 15 m long, the forward photons at the short wavelength ($\leq$ 1540 nm) are reabsorbed, leaving a low floor of the output level which is < -75 dBm in the wavelength range < 1530 nm. In Fig. 6.71(b), the absorption of the main peak is more important in the forward case than in the backward case. In the forward ASE, photons are absorbed as it propagates in the direction of the detector; in the backward ASE, light is amplified instead. But in the regime of near-complete inversion corresponding to high pumps as shown in Fig. 3.12 in Chapter 3, both shapes of ASE spectral become nearly identical, as GSA is

bleached. The photons at the metastable level are being used to amplify the spontaneous emission photons. Therefore, the EDF input end is saturated. With the external injection, the power level decreases due to the backward ASE suppression at the EDF input end. At the low pump power, the rate of the saturation or depopulation induced by the backward ASE is lower than the rate of the backward ASE suppression induced by the moderate level of injection. As a result, the inversion at the EDF input end is restored back to a higher level. This is revealed in the forward ASE spectrum in Fig. 6.71(a) where the spectrum with the injection is higher.

Figs. 6. 72(a) and (b) show the forward and backward ASE spectrum, respectively, for the counter-pumping scheme as shown in Fig. 6.70(b). In this pumping scheme, photons are reabsorbed in the wavelength range < 1575 nm. At the EDFA output, the forward ASE exhibits a decrease in the power level with the existence of the external injection as shown in Fig. 6. 72(a). This will eventually degrade the gain performance. It is worth noting that an increase in the output level is observed in the backward ASE spectrum as shown in Fig. 6.72(b). However, this does not really contribute to the gain enhancement in the EDFA system since the signal is not propagating in this direction. Therefore, the gain enhancement effect is not "seen" by the input signal in the counter-pumping scheme.

With different pumping schemes, the excess pump power was taken as a function of input signal power P_{in} at P_p = 29.4 mW with the signal injected at the resonance as shown in Fig. 6.73. For the small signal P_{in} < -30 dBm, the excess powers for both pumping schemes are basically identical. For P_{in} > -30 dBm, the excess power starts to depart from each other. In the counter-pumping scheme, the excess pump decreases linearly above P_{in} > -20 dBm. In this scheme (see Fig. 6.70(b)), the input signal enters the EDF port at point B where the backward ASE is small.

With a weak pump power at the EDF output end, the strong input signal saturates the gain medium and a lower output spectrum (forward ASE) is obtained as shown in Fig. 6.72(b). The effect of the saturation is that the ground state population will increases with the input signal level. As a result, more pump power will be absorbed, leaving a lower excess power. In the case of co-pumping, the strong backward ASE at the EDF input end at point A as shown in Fig. 6.70(a) is suppressed. Less pump power is being absorbed, thus giving a higher excess power. However, signal-induced saturation limits the efficiency of the backward ASE suppression. In consequence, the excess power does not further increase above $P_{in} > -5$ dBm.

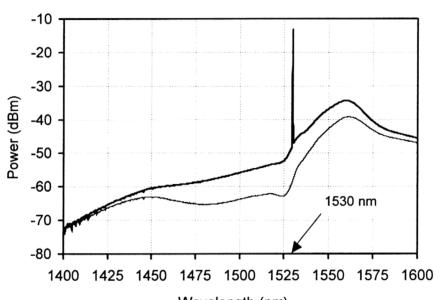

(a)

(continue...)

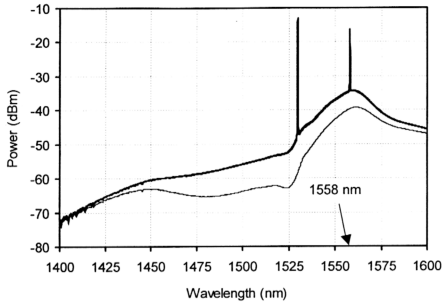

(b)

Fig. 6.62 *Forward ASE spectrum with the pump power of 10.8 mW. Thin line: without injection. Thick line: with injection.*
(a) With injection wavelength of 1530 nm and injection power of –11.8 dBm.
(b) With both injection signal at 1530 nm and probe signal at 1558 nm. Power of probe signal is –30 dBm.

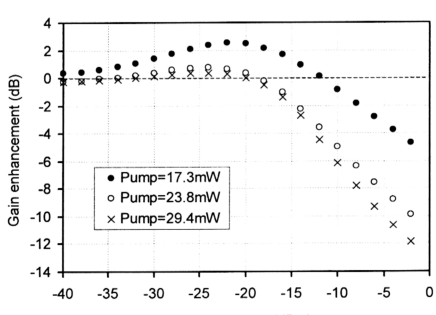

Fig. 6.63 *Gain enhancement of the probe signal as a function of the injection power.*

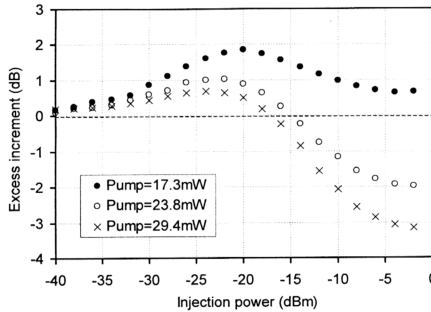

Fig. 6.64 *Increment of excess pump power of the probe signal as a function of the injection power.*

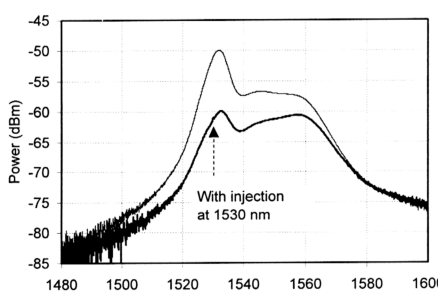

Fig. 6.65 *Backward ASE profile subject to external injection taken from the 1% port of a coupler in the cavity at the pump power of 10.8 mW. (Thin line: without injection; Thick line: with injected signal at the power of –10 dBm and at the wavelength of 1530 nm. A significant suppression of the backward ASE profile is observed.*

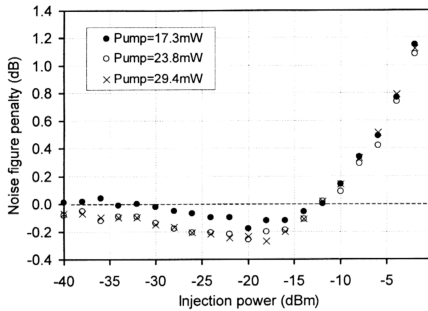

Fig. 6.66 *Noise figure penalty versus injection power. The injection wavelength is 1530 nm.*

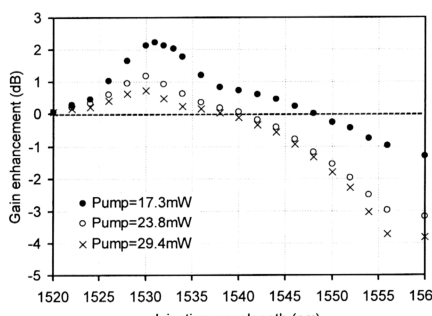

Fig. 6.67 *Gain enhancement versus injection wavelength. The injected signal is fixed at the power of –25 dBm.*

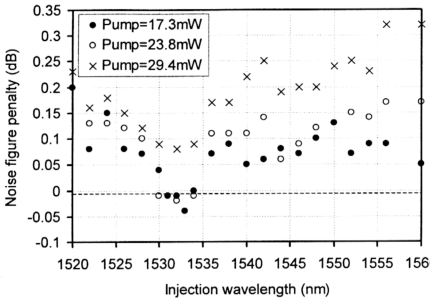

Fig. 6.68 *Noise figure penalty versus injection wavelength. The injected signal is fixed at the power of −25 dBm.*

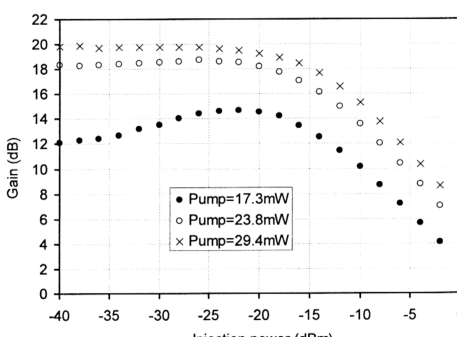

Fig. 6.69 *Gain of injected signal at the wavelength of 1530 nm versus injection power.*

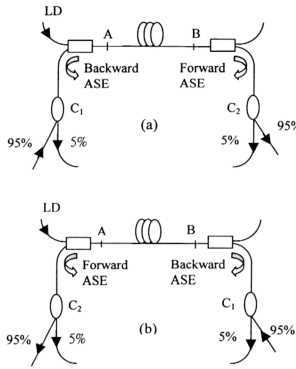

Fig. 6.70 *Experimental setup for measuring the forward and backward ASE for (a) co-pumping, and (b) counter-pumping scheme.*

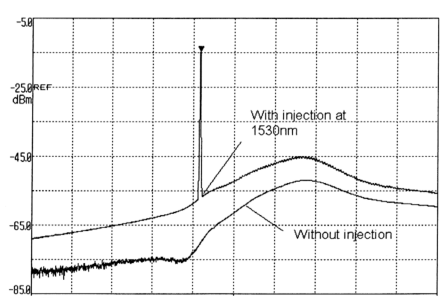

(a) *(continue...)*

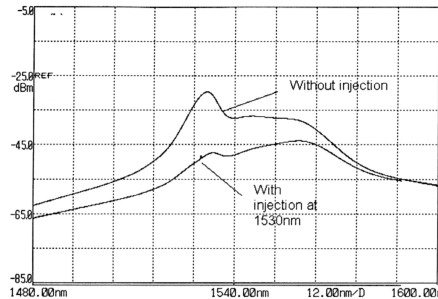

(b)

Fig. 6.71 *(a) Forward and (b) backward ASE spectrum for the co-pumping scheme monitored from the 5% ports of the couplers C_2 and C_1, respectively.*

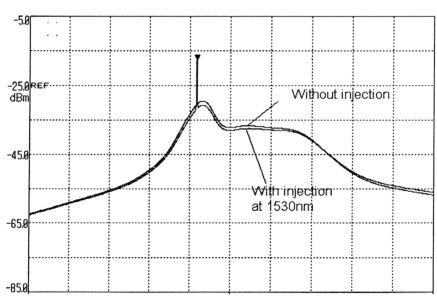

(a) *(continue...)*

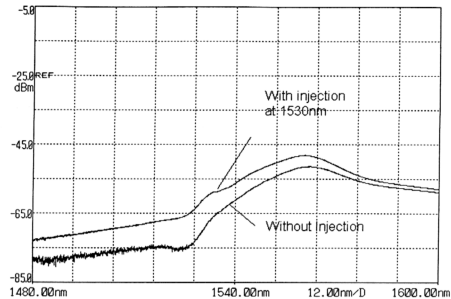

(b)

Fig. 6.72 *(a) Forward and (b) backward ASE spectrum for the counter-pumping scheme monitored from the 5% ports of the couplers C_2 and C_1, respectively.*

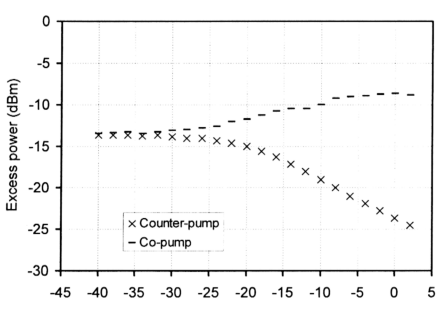

Fig. 6.73 *Excess pump power as a function of input signal power at P_p = 29.4 mW for different pumping schemes. The signal was injected at the resonance.*

6.7 BIDIRECTIONAL–FEEDBACK REGENERATIVE AMPLIFIER

6.7.1 Output Spectrums

In this section, the optical isolator in Fig. 6.1 was removed from the ring cavity. In such a configuration, the ASE traveled in both clockwise and anti-clockwise directions, resulting in oscillation of laser in both directions at the high pump powers. Note that the input signal only circulates in the direction of clockwise. Fig. 6.74(a) shows the output spectrum without input signal at the pump power of P_p = 58.7 mW monitored from the amplifier output port in the clockwise direction. Due to the inhomogeneous broadening of the gain medium, there are two laser modes oscillating in the cavity, at the wavelength of λ_{laser} = 1556 nm and 1559 nm. In the other direction, the spectrum is monitored from the 1 % port of the coupler C_3 as shown in Fig. 6.74(b). There are also two laser modes oscillating in this direction.

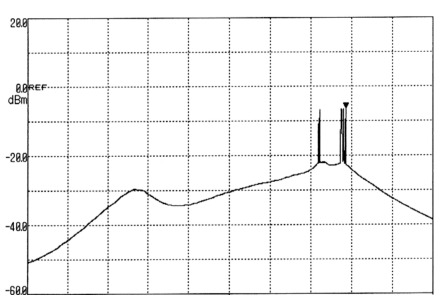

(a)

(continue...)

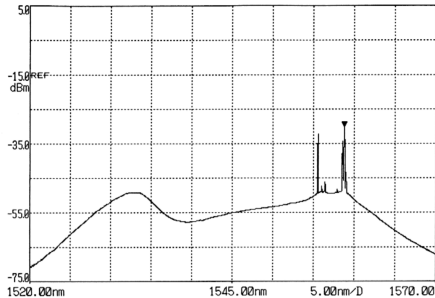

(b)

Fig. 6.74 *Output spectrum without input signal at the pump power P_p = 58.7 mW. (a) in the clockwise direction monitored from the amplifier output port. (b) in anti-clockwise direction monitored from the 1 % port of the coupler C_3.*

6.7.2 Operation Below Threshold

Operating below the oscillation threshold, bidirectional-feedback regenerative EDFA is compared with the unidirectional one. Fig. 6.75 shows the signal gain as a function of below-threshold pump power. The signal at λ_{sig} = 1557.7 nm with the power of P_{in} = -30 dBm was injected into the system. At the low pump powers, the signal gain for both schemes are almost identical since the effect of the feedback is not significant. With the pump increased, the deviation between both schemes increases. The bidirectional-feedback scheme exhibits a signal gain 3.1 dB lower than that of the unidirectional-feedback schemes at P_p = 28.4 mW, just below the oscillation threshold. Note that this threshold pump power is 1 mW lower than the case of unidirectional-feedback. In the bidirectional-feedback scheme, saturation is induced by the ASE in the anti-clockwise directions, resulting in a lower signal gain.

Fig. 6.76(a) shows the noise figure versus pump power at the small signal P_{in} = -30 dBm. Since the backward ASE cannot be effectively suppressed by the small input signal at the EDF input end, the noise figure increases with the pump power in the bidirectional-feedback scheme. The situation becomes worse when the increasing ASE in the anti-clockwise direction is high enough to induce the saturation. For the unidirectional-feedback scheme, the effect of backward ASE increment with the pump power is balanced by the backward ASE suppression induced by the circulating ASE in the clockwise direction. Therefore, the noise figure (~5.5 dB) is lower and independent of the pump power above P_p > 12 mW. This effect is not observed in the bidirectional-feedback scheme since the circulating ASE in the clockwise direction is small due to the saturation induced by the ASE in the anti-clockwise direction. With the saturating signal of P_{in} = -10 dBm, as illustrated in Fig. 6.76(b), the backward ASE is effectively suppressed and thus the inversion level at the EDF input end increases with the pump power. Consequently, the noise figure for both feedback schemes decreases with the pump power.

In Fig. 6.77, the signal gains for both feedback schemes are compared as a function of input signal power P_{in} at the low pump power P_p = 17.3 mW. Due to the saturation induced by the circulating ASE in the anti-clockwise direction in the bidirectional-feedback scheme, the average inversion level is lower. As a result, the small-signal gain is 2.2 dB lower than that obtained in the unidirectional-feedback scheme. At P_{in} = -40 dBm, the signal gain for unidirectional- and bidirectional feedback schemes are 23 dB and 20.8 dB, respectively. The later achieves the saturation input signal power of $\mathcal{L}_{in}^{sat}$ = -17.5 dBm, 2.5 dB higher than the former case.

Noise figure versus input signal power, P_{in} at the low pump P_p = 17.3 mW is illustrated in Fig. 6.78. The saturation effect in the bidirectional-feedback scheme

causes a higher noise figure with an average of ~6 dB in the input power range of –40 $\leq P_{in} <$ -10 dBm. Within this range, the unidirectional-feedback scheme exhibits a noise figure ~0.5 dB lower. Note that the dip is not observed in this plot although both schemes are based on the co-pumping configuration. This is attributed to the relatively low backward ASE at the low pump power. It will be shown in next section that the dip effect is more obvious for the high pump power.

Fig. 6.79 shows the wavelength dependent signal gain at the pump power of P_p = 23.8 mW in the wavelength range of 1540 nm – 1570 nm. With the small signal P_{in} = -30 dBm, the resonant amplification is preserved for both feedback schemes. Resonant gain as high as 29.2 dB is achieved for the unidirectional-feedback scheme and 26.6 dB for the bidirectional-feedback scheme. Due to the circulating ASE in the anti-clockwise direction in the bidirectional-feedback scheme which takes away a portion of the gain, the input signal in the clockwise direction experiences a gain 2.6 dB smaller than the case of unidirectional-feedback at the resonance.

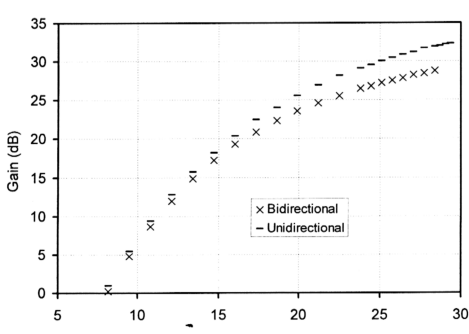

Fig. 6.75 *Signal gain as a function of below-threshold pump power. The signal was injected at λ_{sig} = 1557.7 nm with the power of P_{in} = -30 dBm.*

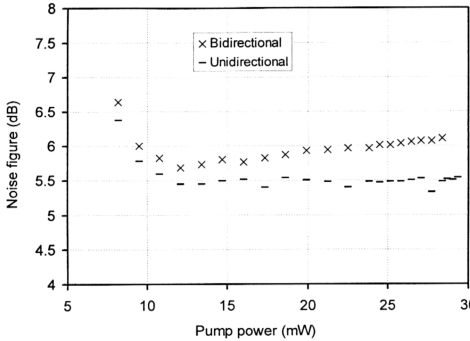

(a)

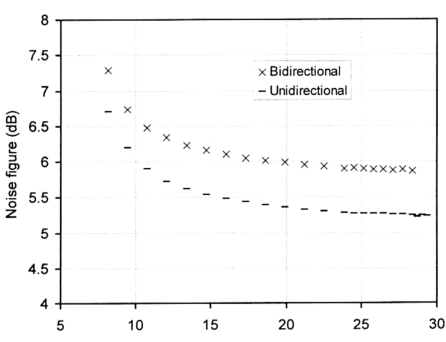

(b)

Fig. 6.76 *Noise figure versus pump power. (a) P_{in} = -30 dBm. (b) P_{in} = -10 dBm.*

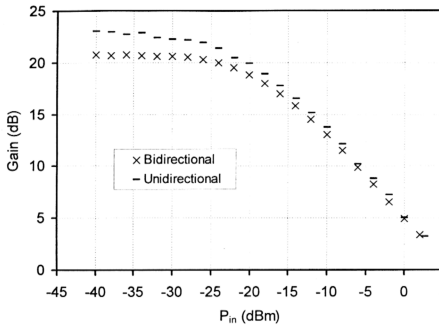

Fig. 6.77 *Signal gain for both feedback schemes are compared as a function of input signal power at P_p = 17.3 mW.*

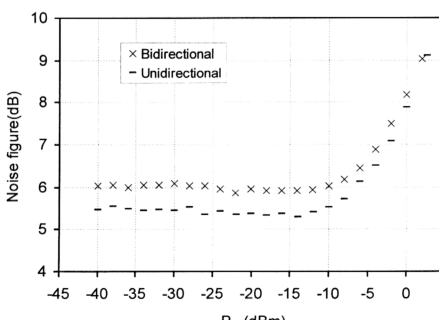

Fig. 6.78 *Noise figure versus input signal power at P_p = 17.3 mW.*

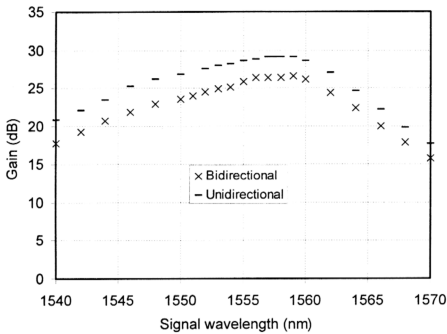

Fig. 6.79 *Wavelength dependent signal gain at P_p = 23.8 mW in the wavelength range of 1540 nm – 1570 nm with the small signal of P_{in} = -30 dBm.*

6.7.3 Operation Above Threshold

In this section, both unidirectional-feedback and bidirectional-feedback regenerative EDFA operating above threshold is presented. Fig. 6.80 shows the signal gain as a function of pump power for both feedback schemes at the small signal of P_{in} = -30 dBm. The systems were characterized at the signal wavelength of λ_{sig} = 1550 nm. Above P_p > 30 mW, the signal gains are nearly independent of the pump power, indicating the gain-clamping effect. Since the bidirectional-feedback system starts to oscillate at a lower pump power (P_p = 28.4 mW), the average inversion is clamped at a lower level. Thus, the signal gain is 3.6 dB lower as compared to the case of unidirectional-feedback which has the threshold pump power 1 mW higher. The maximum gain at the maximum available pump power of 134.5 mW is 30.3 dB and

26.7 dB for the unidirectional- and bidirectional-feedback schemes, respectively. Note that there is still a small gain slope above the lasing threshold especially for the bidirectional-feedback configuration. Such a phenomenon can be attributed to the spectral hole burning effect induced by the oscillating laser. As a result, the population at other sublevels in the metastable level is not completely clamped [28].

Noise figure as a function of pump power for P_{in} = -30 dBm is depicted in Fig. 6.81. In the bidirectional-feedback scheme, the noise figure increases with the pump power whereas the unidirectional-feedback scheme shows an opposite behavior. The noise figure deviates from each other markedly especially at the high pump powers. The deviation increases from 0.9 dB at P_p = 14.1 mW to 2.1 dB at P_p = 134.5 mW. In the co-pumping scheme such as this one, the signal and the pump source enter the same EDF input end where the backward ASE is strong. Saturation effect by the backward ASE is getting stronger with the pump power in such a pumping scheme. Note that the performance of the noise figure is dependent on the population at the EDF input end [8, 29]. Therefore, the noise figure of the small signal should increase with P_p. In Fig. 6.81, this is valid only for the case of bidirectional-feedback. In this case, the backward ASE can be suppressed by a moderately saturated input signal for the co-pumping scheme. With the small signal power of P_{in} = -30 dBm, the increasing oscillating laser with the pump power in the clockwise direction takes over the role of the backward ASE suppression. As a result, the noise figure is expected to decrease with the pump power. However, the oscillating laser in the anti-clockwise direction induces saturation at the EDF input end and cancels the effect of the backward ASE suppression by the oscillating laser in the opposite direction. In consequence, the noise figure increases with the pump power due to the increase in the backward ASE.

Fig. 6.82 shows the dependence of the signal gain on the input signal power P_{in} at the pump power of P_p = 58.7 mW. The unsaturated signal gain for unidirectional- and bidirectional-feedback schemes are ~30 dB and 26.1 dB, respectively. For the former configuration, the gain deviation, ΔG, is relatively large with the maximum ΔG = 1.1 dB in the unsaturated regime. As compared to the case below the oscillation threshold (see Fig. 6.77), the dynamic range increases markedly with the P_{in}^{sat} = -16.1 dBm for the unidirectional-feedback system and –12.5 dBm for the bidirectional-feedback system. Obviously, the bidirectional-feedback scheme exhibits a stronger gain-clamping effect due to the existence of two oscillating laser modes in each direction.

In Fig. 6.83, dependence of noise figure on the input signal power at P_p = 58.7 mW is presented. As compared to the case below threshold, a higher noise figure is exhibited for the case above threshold. In the unsaturated regime, noise figure for the unidirectional- and bidirectional-feedback schemes are ~5.5 dB and ~6.5 dB, respectively. The dip effect is less obvious in the unidirectional-feedback configuration since the backward ASE has already been suppressed by the oscillating laser in the clockwise direction in the unsaturated regime. The depth of the dip for the bidirectional-feedback scheme is limited by the saturation induced by the oscillating laser in the anti-clockwise direction.

Fig. 6.84 shows the amplified output signal power P_{out} versus input signal power, P_{in} at the pump power of P_p = 58.7 mW. The plots differ from that obtained from the conventional single-pass amplifier in which the slope have a sudden change at the input signal power of P_{in} ≈ -16 dBm and –14 dBm for the unidirectional- and bidirectional-feedback systems, respectively. In the above threshold regenerative

amplifier system, these points represent to the condition of injection-locking where oscillating laser in the cavity starts to be locked to the injected signal. In other words, the oscillation starts to oscillate at the wavelength of the input signal. The P_{in} required to lock the unidirectional-feedback system is lower because it experiences a higher gain than that of the bidirectional-feedback system. Above these points, the cavity is dominated by the input signal, leaving only one mode existing in the cavity.

The dependence of the signal gain on the signal wavelength at the P_p = 58.7 mW and the P_{in} = -30 dBm is illustrated in Fig. 6.85. At the resonance, the deviation in the signal gain between unidirectional- and bidirectional-feedback schemes is ~7.5 dB. As compared to the case of below threshold as presented in the previous section, such a discrepancy is relatively large. This can be attributed to the stronger saturation effect in the bidirectional-feedback scheme operating above the oscillation threshold. However, the resonance gain as high as ~ 31 dB is still achievable. The corresponding resonance gain for the unidirectional-feedback scheme is 38.5 dB.

The noise figure is measured as a function of signal wavelength at P_p = 58.7 mW and P_{in} = -30 dBm. The result is illustrated in Fig. 6.86. Both schemes exhibit a large data scattering due to the interference effect arising from the superposition between the input signal and the circulating input signal. This effect can be greatly suppressed with a saturating signal as described in Sec. 6.4.2.3. The unidirectional-feedback achieves a lower noise figure over the amplification bandwidth ranging from 1540 nm to 1570 nm with the average noise figure of ~5 dB whereas the bidirectional-feedback scheme has the noise figure ~1 dB higher.

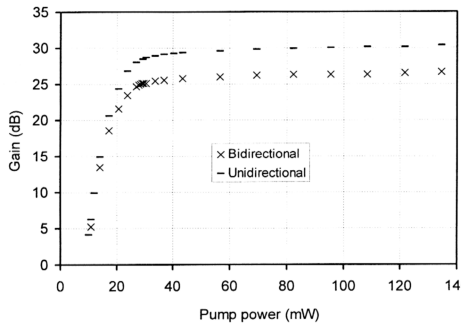

Fig. 6.80 *Signal gain as a function of pump power for both feedback schemes at the small signal of P_{in} = -30 dBm. The systems were characterized at the signal wavelength of λ_{sig} = 1550 nm.*

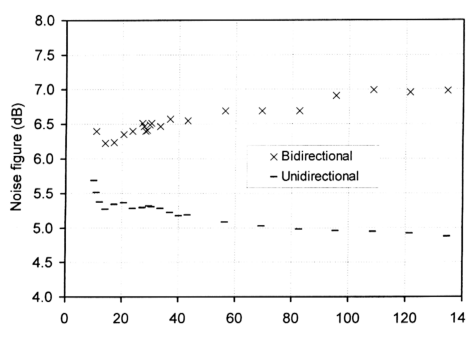

Fig. 6.81 *Noise figure as a function of pump power for P_{in} = -30 dBm.*

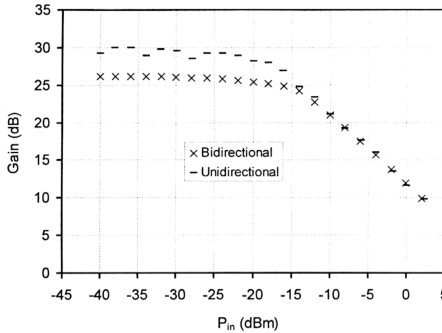

Fig. 6.82 *Dependence of the signal gain on the input signal power at the pump power of $P_p = 58.7$ mW.*

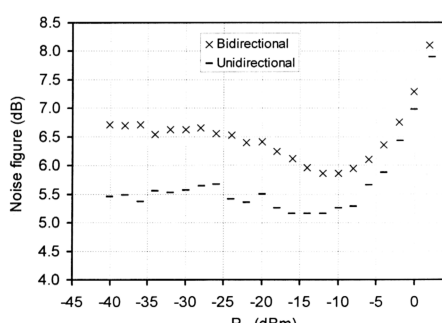

Fig. 6.83 *Dependence of noise figure on the input signal power at $P_p = 58.7$ mW.*

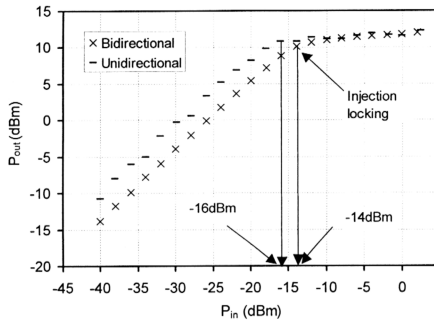

Fig. 6.84 *Amplified output signal power versus input signal power at the pump power of P_p = 58.7 mW.*

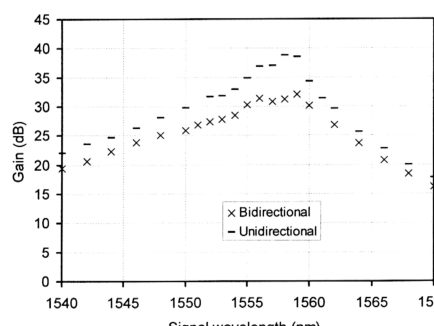

Fig. 6.85 *Dependence of the signal gain on the signal wavelength at P_p = 58.7 mW and P_{in} = -30 dBm.*

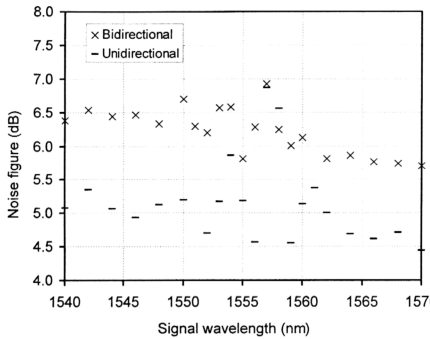

Fig. 6.86 *Noise figure as a function of signal wavelength at P_p = 58.7 mW and P_{in} = -30 dBm.*

6.8 CONCLUSIONS

Erbium-doped fiber amplifier with regenerative-feedback has been presented. Operating below the threshold of self-oscillation, resonant-amplification was found to be preserved for small input signal. Resonant gain as high as 35.1 dB was achieved with the pump power as low as 29.4 mW, just below the oscillation threshold. A flat gain spectral could only be obtained with the saturating input signal. Due to the strong amplification at resonance, the saturation input power was much lower than the case without feedback. Operating above the oscillation threshold, gain-clamping effect was observed. Existence of the oscillating laser effectively suppressed the generation of the backward ASE, thus, increasing the noise performance significantly. However, the application of such a configuration in the optical communication system was severely

deteriorated due to the interference effect. Potential application as a high-power frequency-stabilized laser source was proposed based on the study of injection-locking. An interesting feature was that the gain and noise figure could be improved by injecting another signal with the wavelength ~1530 nm and with a moderate level of power. We proved that such a phenomenon was attributed to the backward ASE suppression instead of attributing the second injection as a secondary pump source. Comparison between unidirectional- and bidirectional-feedback regenerative amplifier showed that saturation induced by the oscillating laser in the anti-clockwise direction degrade the system performance.

REFERENCES

[1] R. J. Freiberg, and C. J. Buczek, "The saturated gain-bandwidth of CO_2 regenerative ring amplifiers," Opt. Commun., 4, pp. 139, 1971.

[2] C. J. Buczek, R. J. Freiberg and M.L. Skolnick, "CO_2 Regenerative Ring Power Amplifiers," J. Appl. Phys., 42, pp. 3133, 1971.

[3] K. Otsuka, "Instabilities in a resonant-type laser amplifier with injected signals," J. Opt. Soc. Am. B, 2, pp. 168, 1985.

[4] T. C. Teyo, P. Poopalan and H. Ahmad, "Regenerative erbium-doped fibre ring laser-amplifier," Electron. Lett., 35 pp. 1471, 1999.

[5] R. G. Smart, J. L. Zyskind, J. W. Sulhoff, and D. J. DiGiovanni, "An Investigation of the Noise Figure and Conversion Efficiency of 0.98 μm Pumped Erbium-Doped Fiber Amplifiers Under Saturated Conditions," IEEE Photon. Technol. Lett., 4, pp. 1261, 1992.

[6] Tuan Chin TEYO, Mun Kiat LEONG and Harith AHMAD, "Noise Characteristics of Erbium-Doped Fiber Amplifier with Optical Counter-Feedback," Jpn. J. Appl. Phys. 41, Part 1, No. 5A, pp. 2949, 2002.

[7] T. C. Teyo, M. K. Leong and H. Ahmad, "Noise Characteristics of Erbium-doped Fiber Amplifier With Different Optical Feedback Schemes," Opt. Comm., 207, pp. 327, 2002.

[8] E. Desurvire, "Erbiun-doped Fiber Amplifiers – Principles and Applications," John Wiley & Sonc, Inc., 1994.

[9] A. E. Siegman, Lasers, University Science Books, CA, 1986.

[10] Y. Kimura and M. Nakazawa, "Laing characteristics of Er^{3+}-doped silica fibers from 1553 up to 1603 nm," J. Appl. Phys., 64, pp. 516, 1988.

[11] T. C. Teyo, N. S. Mohd. Shah, M. K. Leong, P. Poopalan and H. Ahmad, "Comparison between Regenerative-Feedback and Co-Feedback Gain-Clamped EDFA," accepted to be published in IEEE Photon. Technol. Lett., Vol. 4, No. 9.

[12] S. Yamomoto, H. Takahira, E. Shibano, M. Tanaka and Y. C. Chen, "BER performance improvement by forward error correcting code in 5 Gbit/s 9000 km EDFA transmission system," Electron. Lett., 30, pp. 718, 1994.

[13] M. B. Spencer and W. E. Lamb, "Laser with Transmitting Window," Phys. Rev. A. 5, pp. 884, 1972.

[14] H. L Stover, W. H. Steier, "Locking of laser oscillator by light injection," Appl. Phys. Lett., 8, pp. 91, 1996.

[15] J. D. C. Jones, P. Urquhart, "An injection-locked erbium fibre laser," Opt. Comm., 76, pp. 42, 1990.

[16] M. B. Spencer, W. E. Lamb, "Laser with a transmitting window," Phys. Rev. A, 5, pp. 884, 1972.

[17] S. Longhi, "Travelling and standing waves in a laser with an injected signal. Phys. Rev. A, 56, pp. 1553, 1997.

[18] P. Even, K. Ai Ameur, G. M. Stephan, "Modelling of an injected gas laser. Phys. Rev. A, 55, pp. 1441, 1997.

[19] J. R. Tredice, F. T. Arecchi, G. L. Lippi, G. P. Puccioni, "Instabilities in a laser with an injected signal," J. Opt. Soc. Am. B, 2, pp. 173, 1985.

[20] C. J. Buczek, R. J. Freiberg, "Hybrid injection locking of higher power CO_2 lasers," IEEE J. Quantum Electron., QE-8(7), pp. 641, 1972.

[21] Li Huan, T. L. Lucas, J. G. McInerney, M. W. Wright, R. A. Morgan, "Injection locking dynamics of vertical cavity semiconductor lasers under

conventional and phase conjugate injection," IEEE J. Quantum Electron., QE-32(2), pp. 227, 1996.

[22] W. Chow Weng, "Theory of line narrowing and frequency selection in an injection locked laser," IEEE J. Quantum Electron., QE-19(3), pp. 243, 1983.

[23] B. J. Feldman, M. S. Feld, "Laser-induced line-narrowing effects in coupled Doppler-broadened transition. II. Standing-wave features," Phys. Rev. A, 5, pp. 899, 1972.

[24] G. M. Stephan, "Spectral properties of an injected laser," Phys. Rev. A , 58, pp. 2467, 1998.

[25] T. C. Teyo, V. Sinivasagam, M. K. Abdullah, H. Ahmad, "An injection-locked erbium-doped fibre ring laser," Opt. & Laser Technol., 31, pp. 493, 1999.

[26] D. J. Jones and O. K. Bandy, "Attractors and chaos in the laser with injected signal," J. Opt. Soc. Am. B, 7, pp. 2119, 1990.

[27] M. A. Mahdi, F. R. Mahamad Adikan, P. Poopalan, S. Selvakennedy, W.Y. Chan and H. Ahmad, "Long-wavelength EDFA gain enhancement through 1550 nm band signal injection," Opt. Comm., 176, pp. 125, 2000.

[28] M. F. Krol, Y. Liu, J. J. Watkins and M. J. Dalley, "Gain Variation in Optically Gain Clamped Erbium Doped Fiber Amplifiers." ECOC'98, pp. 43, 1998; M. F. Krol, Y. Q. Liu, J. J. Watkins and D. W. Lambert, "Dual cavity optical automatic gain control for EDFA," OFC/IOOC '99. Technical Digest , 2, pp. 214 , 1999.

[29] M. Cai, X. Liu, J. Cui, P. Tang, and J. Peng, "Study on noise characteristic of gain-clamped erbium-doped fiber-ring lasing amplifier," IEEE Photon. Technol. Lett., 9, pp. 1093, 1997.